Journal of Performance of Constructed Facilities. Submitted September 20, 2013; accepted January 22, 2014; posted ahead of print January 25, 2014. doi:10.1061/(ASCE)CF.1943-5509.0000585

PERFORMACE OF BURIED TUNNELS SUBJECTED TO SUFRACE BLAST INCORPORATING FLUID STRUCTURE INTERACTION

Koneshwaran Sivalingam[1], David P. Thambiratnam[2], Chaminda Gallage[3]

Abstract

This paper uses finite element techniques to investigate the performance of buried tunnels subjected to surface blasts incorporating fully coupled Fluid Structure Interaction and appropriate material models which simulate strain rate effects. Modelling techniques are first validated against existing experimental results and then used to treat the blast induced shock wave propagation and tunnel response in dry and saturated sands. Results show that the tunnel buried in saturated sand responds earlier than that in dry sand. Tunnel deformations decrease with distance from explosive in both sands, as expected. In the vicinity of the explosive, the tunnel buried in saturated sand suffered permanent deformation in both axial and circumferential directions, whereas the tunnel buried in dry sand recovered from most of the axial deformation. Overall, response of the tunnel in saturated sand is more severe for a given blast event and shows the detrimental effect of pore water on the blast response of buried tunnels. The validated modelling techniques developed in this paper can be used to investigate the blast response of tunnels buried in dry and saturated sands.

Keywords: Explosion, tunnel, Fluid Structure Interaction, material models, saturated sand, strain rate effects, centrifuge test, Finite Element modelling

---

1. Faculty of Science & Engineering, Queensland University of Technology, GPO Box 2434, 2 George St., Brisbane, Queensland 4001. E-mail: sivalingam.koneshwaran@qut.edu.au.

2. Professor, Faculty of Science & Engineering, Queensland University of Technology, GPO Box 2434, 2 George St., Brisbane, Queensland 4001. E-mail: d.thambiratnam@qut.edu.au.

3. Lecturer, Faculty of Science & Engineering, Queensland University of Technology, GPO Box 2434, 2 George St., Brisbane, Queensland 4001. E-mail: chaminda.gallage@qut.edu.au.

Journal of Performance of Constructed Facilities. Submitted September 20, 2013; accepted January 22, 2014; posted ahead of print January 25, 2014. doi:10.1061/(ASCE)CF.1943-5509.0000585

Introduction

Transit tunnels are often constructed at shallow depths and the surrounding media such as soil and rock constrain the tunnels from any relative movement. Despite being stable under geostatic conditions, the response of buried structures to impulsive loads, such as bomb blasts, is dynamic as damping from the surrounding medium is insignificant. The shock wave from an explosion reaches the structure in a very short time, before the damping activates itself (Shin et al. 2011). As a result, excessive stresses and strains caused by the shock wave affect the structural integrity of tunnel lining leading to a localized failure and potential collapse of the tunnel with serious consequences. This highlights the need to investigate the vulnerability of transit tunnels to bomb attacks.

Explosion induced tunnel response results from different phases such as ground shock, Soil Structure Interaction (SSI) and response of tunnel lining. The ground shock continues until the shock waves completely attenuate in the soil. Under geostatic conditions, the effects of SSI on the response of tunnels vary with the confining stress field. When the shock wave intercepts the geostatic SSI, the interface between the tunnel and surrounding soil experiences an inertia effect which lasts for a few milliseconds for explosion-induced ground shock.

The four main factors which influence the response of tunnels under ground shock include: (i) surrounding medium (geological and geotechnical condition), (ii) explosive weight, (iii) distance between explosive and tunnel and (iv) stiffness of tunnel lining. Nature and circumstances determine the first three factors, but the fourth factor is the engineer's choice. Underground engineers can investigate the vulnerability of tunnel-stiffness under different scenarios and offer appropriate designs/retrofits to protect the tunnels from ground shock.

Journal of Performance of Constructed Facilities. Submitted September 20, 2013; accepted January 22, 2014; posted ahead of print January 25, 2014. doi:10.1061/(ASCE)CF.1943-5509.0000585

In this research field, there are no records on full-scale prototype field experiments that study the response of tunnels under surface blast loading. However, some research has been conducted using both scaled-down centrifuge tests and explicit nonlinear finite element techniques.

Full-scale field tests using real tunnels are extremely risky and expensive, but tests on reduced scale models with geotechnical centrifuge are feasible to investigate the blast effect on underground structures. Researchers, Whittaker (Whittaker 1987), Kutter et al. (Kutter et al. 1988) and Davies (Davies 1994), employed the centrifuge modelling technique to study the response of tunnels under explosion, and concluded that the centrifuge test provided a valid technique for investigating response of buried structures. A series of studies had been conducted using centrifuge tests to investigate the surface blast effects on underground structures where a copper pipe (tunnel) was buried in dry sand (De 2012; De et al. 2013; De and Zimmie 2006; De and Zimmie 2007). These experiments provide quantitative information on the effects of surface explosion on the tunnel buried in sand.

Yang et al. (Yang et al. 2010) conducted a numerical simulation of the blast response of a metro tunnel in Shanghai using an advanced general purpose multi-physics simulation software LS-DYNA (LSTC. 2007). They used Arbitrary Lagrangian-Eulerian (ALE) method where Eulerian meshes were used for air, soil and explosive while Lagrangian mesh was employed for the tunnel. Merged nodes at the interface of the two parts facilitated the stress transfer between the soil and the tunnel. Feldgun et al. (Feldgun et al. 2008) investigated the soil-structural separation of a buried tunnel subjected to internal explosion. The comparison of analysis with and without soil-structural separation shows a significant variation in the

Journal of Performance of Constructed Facilities. Submitted September 20, 2013; accepted January 22, 2014; posted ahead of print January 25, 2014. doi:10.1061/(ASCE)CF.1943-5509.0000585

tunnel response. Olarewaju (Olarewaju 2012 (a); Olarewaju 2012 (b); Olarewaju 2013) describes a recent series of numerical studies that had been carried out on buried pipes to investigate the pipe response due to accidental explosions using the commercial Finite Element program ABAQUAS. In this study, the interaction be- tween the soil and pipe was simulated by perfectly bonded 'no slip' condition which may be appropriate for small pipe structures as the pipe deforms with soil in which case separation and sliding effects of the interface are negligible. For large tunnel structures, it is vital to incorporate the contact model that allows separation, recontact and sliding.

Olarewaju (Olarewaju 2012 (a); Olarewaju 2012 (b); Olarewaju 2013) simplified the soil and pipe materials to be a linear, homogeneous and isotropic. This assumption may be valid for far field blast and subsequent structural response, but the behaviour of soil and resistance of pipe material under blast loading are highly nonlinear. In addition, the material models should include strain rate effects.

Gui and Chien (Gui and Chien 2006) investigated a bored tunnel passing beneath Taipei Shongsan airport under buried explosion. Their model employed the Finite Difference software FLAC^{2D} with a simplification of three dimensional (3D) blast waves into a two dimensional (2D) blast wave. It was a conservative approach, though it considerably minimized the computation cost. The model also simulated the soil-tunnel interface with static and dynamic frictions in order to permit the sliding. Liu (Liu 2009; Liu 2012) investigated the dynamic response of subway tunnels subjected to internal blast using the computer code ABAQUAS, where the cast iron tunnel was modelled as a shell structure, assuming a triangular blast pressure on the internal surface of the tunnel. Although the focus

Journal of Performance of Constructed Facilities. Submitted September 20, 2013; accepted January 22, 2014; posted ahead of print January 25, 2014. doi:10.1061/(ASCE)CF.1943-5509.0000585

of the study was on the SSI and stiffness of the lining, the simulation did not consider the important aspect of air-structural interaction, a 3D blast effect and direct heat effect from the internal blast. The heat effect may not be very important to the buried tunnels subjected to surface blast as the surrounding soil medium will act as a good heat insulation material. When an explosive detonates in contact with the ground, the blast waves propagate hemi-spherically in the ground and affect the performance of structures in all directions. This emphasizes the need for 3D analysis in order to simulate a more realistic problem (Higgins 2011). The 3D analysis requires considerable computational time and large memory. Application of an effective modelling technique greatly reduces the computation time and memory.

Using the centrifuge test results, De (De 2012) validated his numerical model developed from AUTODYN. Eulerian meshes were used to model the air and explosive while the soil and the copper-tunnel were modelled with Lagrangian meshes. Penalty based interaction 'Lagrange-Lagrange' method simulated the interface between the soil and tunnel. He utilised a default sand model based on a publication by Laine and Sandvik (Laine and Sandvik 2001). The material model simulates the strain rate behaviour of sand (Higgins et al. 2012). Soil moisture content has a significant influence on the response of buried structures under blast loads. To date, no one has studied the effects of pore water pressure in the soil for the blast response of underground tunnels. De (De 2012) also highlighted the need for soil models to incorporate pore water effects.

Numerical simulations have various limitations, such as lack of appropriate material models and relevant material parameters, which impede the progress of the numerical studies. This

Journal of Performance of Constructed Facilities. Submitted September 20, 2013; accepted January 22, 2014; posted ahead of print January 25, 2014. doi:10.1061/(ASCE)CF.1943-5509.0000585

paper treats the response of a buried tunnel subjected to surface explosion using finite element techniques, incorporating fully coupled Fluid Structure Interaction (FSI) and appropriate material models for air, explosive, soil and tunnel. It utilises the '*MAT_FHWA_SOIL' material model (Lewis 2004) which can simulate dry, partially saturated and fully saturated soil conditions. In addition, the material model includes strain rate effects, strain softening, kinematic hardening and element deletion. Laboratory tests and/or equations in the material manual (Lewis 2004) allow to evaluate the material parameters. The copper material model used for the buried tunnel also incorporates the strain rate effect which is essential due to wave propagation through the copper tunnel (Peroni et al. 2009). Results from the numerical analysis of dry sand are validated with known results reported in (De 2012; De and Zimmie 2006). The study further investigated the blast response of the tunnel buried in saturated sand.

Numerical Approaches for Blast Analysis

Hydrocodes are the computational tools that can be used to solve wide range of non-linear problems in solid, fluid flow and explosions. There are several numerical techniques available in hydrocodes, but selection of an appropriate numerical technique is wholly dependent on type of problem and computational cost. In the present study, explosion occurs just above the ground where only blast waves compress the ground surface. The compressed blast wave produces a crater which is always smaller than a crater from a buried explosion (Ambrosini et al. 2003). In numerical simulation, the crater formation occurs by compressing the finite elements downwards, in which case element deletion algorithm may not be necessary. Large deformations are inherent in soil-explosion problems. Different numerical techniques available in LS-DYNA, such as Arbitrary Lagrangian-Eulerian-ALE (Shared

Journal of Performance of Constructed Facilities. Submitted September 20, 2013; accepted January 22, 2014; posted ahead of print January 25, 2014. doi:10.1061/(ASCE)CF.1943-5509.0000585

nodes between Lagrangian and Eulerian), Smooth Particle Hydrodynamics (SPH) and Fluid Structural Interaction-FSI (ALE/Lagrangian Coupling) are capable of handling problems with large deformations. The numerical simulations divide the system into finite elements, a process called discretisation. The discretisation takes place with respect to time (temporal) and space (spatial). In numerical simulations, temporal discretisation uses the explicit method which calculates the state of a system at a later time as a function of time step from the current state of the system. In order to capture any activity within an element, the time step should satisfy the Courant-Friedrich-Levy (CFL) condition for which the time step (Δt) is less than the duration for sound to cross the smallest element. Usually, it is advised to use a Safety Factor (SF) of 0.67 for blast loads in LS-DYNA, which could be different for other computer software. This condition can be generally expressed as below:

$$0 < \Delta t \leq N \frac{l}{c} \qquad \text{Eq. 1}$$

where N is the safety factor, l is the least element size and c is the sound speed through the element.

Different types of spatial discretisation solvers are available to model various materials and their conditions, utilising the suitable features of each solver. Lagrangian solver is used in the finite element method, in which the elements move with the material during the deformation. There is no flow of material from one element to the other. This solver is more suitable for solid objects where the deformation is addressed by the distortion of the mesh. For large deformation problems, this solver undergoes severe element distortion which may result in very small time steps (Δt) and grid tangling. Eulerian solver is used in the finite difference method and/or finite volume method, in which the mesh remains undeformed while the material flows freely from one to another element. This solver is most suitable for fluid

Journal of Performance of Constructed Facilities. Submitted September 20, 2013; accepted January 22, 2014; posted ahead of print January 25, 2014. doi:10.1061/(ASCE)CF.1943-5509.0000585

materials such as a gas or a liquid. Eulerian solver can also be used to model solid objects where larger deformation is inevitable, but this solver is very difficult to deal with the material boundary conditions involving surface slippage in contact (Wang et al. 2005).

Shortcoming of both pure Lagaranian and pure Eulerian techniques are eliminated by introduction of ALE technique which is capable of solving problems, combining the best features of both the Lagrangian and the Eulerian solvers. In ALE, the nodes in the computational mesh may be moved with the continuum in Lagrangian manner, or held fixed as in Eulerian manner, or moved in some arbitrarily specified way to give a continuous rezoning capability. With this feature of freedom to move the computational mesh, the ALE efficiently handles the problem with greater distortions of the mesh than the purely Lagrangian method. It also offers more resolution than the purely Eulerian method. However, considering the increase in computational time for the simulation, this technique has become less attractive. In order to reduce the computational time, Eullerian solvers are used to model the effect of explosion on near field material while using Lagrangian solvers for the far field material. This technique requires a form of interaction between those Eulerian and Lagragian meshes. The interaction is achieved by merging the common nodes at their juncture. This technique is applicable if the targeted structure is sufficiently away from the explosion. If it does not comply, severe mesh distortion will occur in Eulerian mesh next to the Lagrangian mesh. Consequently, sharp reduction of the time step will cause incomplete simulation. Jayasinghe et al. (Jayasinghe et al. 2013) recently used this method to simulate the underground explosion and subsequent response of pile foundation.

Meshless methods such as Smooth Particle Hydrodynamics (SPH) (Wang et al. 2005) prevent

Journal of Performance of Constructed Facilities. Submitted September 20, 2013; accepted January 22, 2014; posted ahead of print January 25, 2014. doi:10.1061/(ASCE)CF.1943-5509.0000585

the aforementioned difficulties of small time steps and grid tangling by employing explicit nodal connectivity. The SPH allows the nodes to move about the domain in a Lagrangian style and interactions between nodes are controlled as part of the computation. Accurate SPH simulations require uniformly sized large number of SPH particles throughout the SPH region to reproduce the hydrodynamic behaviour of the loading on the structure. Furthermore, the interaction of nodes without an explicit mesh makes the simulation computationally expensive. Similar to ALE-shared node approach, a coupled SPH and Finite Element Method (FEM) (Wang et al. 2005) is effective for modelling the process involving large deformations caused by the explosion, shock wave propagation and the response of structures. The basic concept of interaction between the SPH and Lagrange FEM is formed by joining them. Some researchers (Barsotti et al. 2012; Wang et al. 2005) have successfully used the SPH method to simulate a buried explosion. Simulation of an explosion in air and subsequent response of the buried structure are complicated with SPH as the surrounding air domain has to be modelled with SPH particles for more accurate solution (Koneshwaran et al. 2013). Though the SPH method has very attractive features, it does suffer from a numerical problem called tensile instability which could result in particle clumping or complete blowup in the computation. The clumping of the SPH particles is unrealistic and needs to be prevented in a real solid by introducing a repulsive force between the particles (Monaghan 2000), which requires the involvement of experts.

Fluid-Structure Interaction (FSI) is a multi-physics simulation process for solving highly non-linear transient problems with large deformations of structures such as those caused by an explosion. It enables to model the surrounding air and explosive using separate ALE meshes (background meshes) while Largrangian meshes are used to model the deformable structural

Journal of Performance of Constructed Facilities. Submitted September 20, 2013; accepted January 22, 2014; posted ahead of print January 25, 2014. doi:10.1061/(ASCE)CF.1943-5509.0000585

parts. In the FSI, the computation searches for the intersections between the ALE and Lagrangian parts. If a coupled Lagrangian surface is detected inside an ALE domain, the coupling algorithm computes the penetration of the ALE material across the Lagrangian surface. During every computational step, the interaction forces are calculated for their resultant penetration of both materials. Although the ALE-Lagrangian coupling computation is expensive, effective handling of model throughout the simulation will significantly reduce the computational cost in LS-DYNA using restart option. In the present study, FSI (ALE/Lagrangian Coupling) approach is considered to be most effective for simulating the above ground explosion and subsequent structural response of the buried tunnel.

Material Constitutive Models

This paper studies the blast response of a copper tunnel (pipe) buried in sand using LS-DYNA and compares the results with those from centrifuge tests (De 2012; De and Zimmie 2006). In this simulation, the following material models are considered for modelling air, explosive, soil and tunnel (copper):

Air

The air is modeled as an ideal gas (LSTC. 2007) utilising '*MAT_NULL material model with a linear polynomial Equation of State (EOS). The pressure is expressed by:

$$P = C_0 + C_1\mu + C_2\mu^2 + C_3\mu^3 + \left(C_4 + C_5\mu + C_6\mu^2\right)E \qquad \text{Eq. 2}$$

Where E is the internal energy per unit volume, C_0, C_1, C_2, C_3, C_4, C_5, and C_6 are constants and $\mu = \frac{\rho}{\rho_0} - 1$, where $\frac{\rho}{\rho_0}$ is the ratio of current density to initial density.

Journal of Performance of Constructed Facilities. Submitted September 20, 2013; accepted January 22, 2014; posted ahead of print January 25, 2014. doi:10.1061/(ASCE)CF.1943-5509.0000585

The linear polynomial equation represents an ideal gas with the gamma law EOS, in which $C_0=C_1=C_2=C_3= C_6= 0$ and $C_4 = C_5= \gamma -1$, where γ is the ratio of specific heat at constant pressure per specified heat at constant volume. The pressure is then described by:

$$P = (\gamma -1)\frac{\rho}{\rho_0} E_0 \quad \text{Eq. 3}$$

where: $$E_0 = \rho_0 c_v \times T \quad \text{Eq. 4}$$

γ is an adiabatic constant for air behaving as an ideal gas (estimated value for γ =1.4), ρ is the density, c_v is the specific heat at constant volume and E_0 is the initial internal energy per unit volume. Table 1 shows the material parameters used for the air.

Explosive

The Jone-Wilkin-Lee's EOS is used to describe the explosive as it is the most popular one and the easiest to calibrate. This EOS defines the pressure as below:

$$P = A\left(1-\frac{\omega}{R_1 V}\right)e^{-R_1 V} + B\left(1-\frac{\omega}{R_2 V}\right)e^{-R_2 V} + \frac{\omega E}{V} \quad \text{Eq. 5}$$

In the above equation ***V*** is the relative volume or the expansion of the explosive, ***E*** is the initial energy per volume, ***A, B, R_1, R_2*** and ***ω*** are empirically derived constants for the explosive. Table 2 shows the material parameters used for both TNT (Trinitrotoluene) explosives.

Soil

This research uses an appropriate soil model that incorporates the various soil compositions, in particular, moisture content. By evaluating several material models in LS-DYNA, *MAT_FHWA_SOIL model was identified as a suitable soil model that includes strain

Journal of Performance of Constructed Facilities. Submitted September 20, 2013; accepted January 22, 2014; posted ahead of print January 25, 2014. doi:10.1061/(ASCE)CF.1943-5509.0000585

softening, kinematic hardening, strain rate effects, element deletion, excess pore water effects and stability with no soil confinement (Lewis 2004; Saleh and Edwards 2011). The material model was developed by the Federal Highway Administration (FHWA) in 2004. The FHWA soil model is based on a modified Mohr-Coulomb yield criterion (Abbo and Sloan 1995). The modified yield surface is a smooth hyperbolic surface which enables an accurate, robust, and a significant computational saving of numerical simulation.

This material model requires main parameters such as, mass density, specific gravity, bulk modulus, shear modulus and moisture content. These soil parameters are generally determined through laboratory tests. Parameters required for defining strain softening, kinematic hardening, strain rate effects and pore water effects can be evaluated through laboratory tests and/or equations in the material manual (Lewis 2004).By considering the pore-water effect, Lee (Lee 2006) and Jayasinghe et al. (Jayasinghe et al. 2013) successfully employed the model for studying blast induced liquefaction in fully saturated soil. If the soil is unsaturated or dry, the same model can be utilised by eliminating pore-water effects (Lee 2006). Saleh and Edwards (Saleh and Edwards 2011) also used this model for investigating the interaction of landmine explosion with protective structures by ignoring the pore-water effects.

At the outset of the Civil and Mechanical Systems Program of the National Science Foundation (NSF), Nevada sand (at a relative density (D_r) of 60%) was used for centrifuge tests by De (De 2012). In 1992, Arulmoli et al. (Arulmoli et al. 1992) conducted an extensive laboratory test for the Nevada sand with different D_r values including: 40% and 60% in the VELACS (Verification of Liquefaction Analyses by Centrifuge Studies) Program.

Journal of Performance of Constructed Facilities. Submitted September 20, 2013; accepted January 22, 2014; posted ahead of print January 25, 2014. doi:10.1061/(ASCE)CF.1943-5509.0000585

From Cyclic Triaxial Test data for Nevada sand at D_r = 60% (Arulmoli et al. 1992), the main soil parameters such as mass density (ρ), specific gravity (G_s) and moisture content were reported as 1.6g/cm^3, 2.67 and 0 respectively. Based on initial void ratio, porosity of the sand was derived as 0.4. De (De 2012) presented data for density (ρ) versus sound speed (c) that was used for back-calculation of shear modulus (G). The velocities of primary wave (V_P) and shear wave (V_S) depend on the compressibility of the soil body through Eq.6 (Kramer 1996).

$$\frac{V_P}{V_S} = \sqrt{\frac{2-2v}{1-2v}} \qquad \text{Eq. 6}$$

where v is the Poisson's ratio of soil.

For Nevada sand v = 0.33 (De 2012) and the ratio V_P/V_S = 1.985. Using this ratio of V_P/V_S, the shear wave velocity (V_S) can be calculated using Eq.7 for known initial sound speed (c) at initial mass density of 1.6 g/cm^3.

$$V_S = \sqrt{\frac{3(V_P^2 - c^2)}{4}} \qquad \text{Eq. 7}$$

From Eq.8 (Kramer 1996), the shear modulus (G) was calculated as 56.0 MPa, which is consistent with the shear modulus evaluated from resonant column test for Nevada sand at D_r = 60% (Arulmoli et al. 1992). In the VELACS project, degradations of Shear Modulus were graphically described by the variation of the shear modulus with shear strain. Although the variation is significant to represent the non-linear characteristics of soil, the *MAT_ FHWA_SOIL soil model assumes a constant shear modulus in its calculation. Lee (Lee 2006) suggested that LS-DYNA's restart feature can offer an option to alter the shear modulus during the blast simulation.

Journal of Performance of Constructed Facilities. Submitted September 20, 2013; accepted January 22, 2014; posted ahead of print January 25, 2014. doi:10.1061/(ASCE)CF.1943-5509.0000585

$$G = \rho V_S^2 \quad \text{Eq. 8}$$

The Bulk modulus (K) was derived as 146.0 MPa from shear modulus (G) and Poison's ratio v using Eq.9.

$$K = \frac{2G(1+v)}{3(1-2v)} \quad \text{Eq. 9}$$

The *MAT_FHWA_SOIL soil model handles pore water pressure build-up using the relationship between pore-water pressure (u) and volumetric compression strain (ε_v) as shown in Eq.10. (Lewis 2004).

$$u = \frac{K_{sk}}{1 + K_{sk} D_2 n_{cur}} \varepsilon_v \quad \text{Eq. 10}$$

where K_{sk} = skeleton bulk modules, n_{cur} = current porosity due to air voids and D_2 = a function of Skempton's pore-water pressure.

Eq.11 defines the parameter D_2 from Skempton pore-water pressure parameter B, as shown below:

$$B = \frac{1}{1 + n\frac{K_{sk}}{K}}, \qquad D_2 = \frac{1-B}{BK_{sk}[n(1-S)]} \quad \text{Eq. 11}$$

where n = soil porosity and S = degree of saturation.

The parameter D_2 is constant for partially saturated soil. For fully saturated case, the constant D_2 has no effect on pore-water pressure (i.e $D_2 = 0$) (Lee 2006).

Aforementioned shear (G) and bulk (K) moduli were obtained for the Nevada sand in dry condition. Inclusion of water will change those magnitudes with level of saturation as the water is nearly incompressible with high bulk modulus and negligible shear modulus. Shear

Journal of Performance of Constructed Facilities. Submitted September 20, 2013; accepted January 22, 2014; posted ahead of print January 25, 2014. doi:10.1061/(ASCE)CF.1943-5509.0000585

modulus of saturated soil can be computed from both saturated density (ρ_{sat}) and shear wave velocity (V_{S-sat}) for saturated soil using Eq.12. Ernest Naesgaard et al. (Naesgaard et al. 2007) reported that the shear wave velocity (V_S) is essentially independent of the Skempton parameter *B*. Therefore the saturated shear modulus (G_{sat}) can be assumed to be the same as the dry shear modulus (G).

$$G_{sat} = \rho_{sat} V_{S-sat}^2 \qquad \text{Eq. 12}$$

From comparison of primary wave velocity (V_P) versus Skempton parameter B (Naesgaard et al. 2007), it is observed that the primary wave velocity (V_P) varies between 1200 ms^{-1} and 1500 ms^{-1} when the Skempton parameter *B* is close to 1.00. In the VELACS project, the Skempton parameter *B* was obtained as 0.98 for sand at D_r = 60%. The value of the saturated bulk modulus can then be found from Eq.13.

$$K_{sat} = \rho_{sat} V_{P-sat}^2 - \frac{4}{3} G_{sat} \qquad \text{Eq. 13}$$

where $V_{P\text{-}sat}$ is the primary wave velocity in saturated soil.

Copper (pipe material)

The copper tunnel is modelled using *MAT_PLASTICIY_KINEMATIC material model which incorporates both non-linear material behaviour and high strain rate effects due to the ground shock. Material parameters for copper (Matuska 1984; Peroni et al. 2009) are described in Table 3. The main parameters include mass density (ρ), young's modules (E), poisson's ratio (υ), yield stress (σ_y), tangent modules (E_{tan}), hardening parameter (β) and strain rate parameters (C) & (P) for Cowper Symonds strain rate model.

Journal of Performance of Constructed Facilities. Submitted September 20, 2013; accepted January 22, 2014; posted ahead of print January 25, 2014. doi:10.1061/(ASCE)CF.1943-5509.0000585

Numerical Model

Problem description

Centrifuge testing is useful for testing small-scale models to simulate the same physical behaviour in the soil as in large-scale nonlinear problems. This numerical study simulates an experiment conducted by De (De 2012) using a 70 g centrifuge testing machine, where g is the gravitational acceleration. He investigated a tunnel response using scaled-down models subjected to a surface blast. The scaled-down model composed of a copper tunnel buried in dry Nevada sand (a relative density (D_r) = 60%) at a depth of 3.6 m equivalent to prototype scale as shown in Fig. 1. A spherical shape explosive was symmetrically placed above the midspan, directly over the centerline of the copper tunnel, such that the ground surface was tangent to the spherical surface of the explosive.

The copper tunnel was instrumented with 19 strain gauges to monitor axial, circumferential and shear strains at different locations on the tunnel. For comparison purpose, three gauge readings reported in (De 2012; De and Zimmie 2006) were considered. Fig. 13 describes the corresponding gauge locations in the prototype model.

Centrifuge scaling factors show how a field model and its dynamic events are correlated in the centrifuge test, in which the scaled model is sufficiently raised to N times the gravitational acceleration. Scaling factors for different parameters are shown in Table 4. Based on the centrifuge scaling laws, Table 5 lists the corresponding prototype model dimensions for the numerical simulation.

Journal of Performance of Constructed Facilities. Submitted September 20, 2013; accepted January 22, 2014; posted ahead of print January 25, 2014. doi:10.1061/(ASCE)CF.1943-5509.0000585

Details of modelling

Symmetric modelling capabilities play important roles in this numerical simulation to reduce the computational cost by considering a quarter symmetry-geometrical prototype models with a size of 20 m x 16 m x 15 m as shown in Fig. 2. This prototype model was used to represent the Lagrangian structure which is composed of only two major parts: copper tunnel and soil. Eight-node solid elements are used with different spatial discretisation solvers. Lagrangian meshes are used to model the soil and copper tunnel while ALE meshes (background mesh) are used separately to model the surrounding air and explosive. A mesh consistency condition is achieved through a series of cases with different meshes to capture the analytical solution in the limit of a mesh refinement process. The Lagrangian soil structure uses smaller element size of 12.5 cm x 12.5 cm x 12.5 cm in the region adjacent to the explosive and larger element size of 40 cm x 40 cm x 40 cm for far field region.

The copper tunnel is modelled with due consideration for a greater mesh refinement of curved surfaces. Peaks and valleys on the curved surface of copper tunnel interlock with interface of soil elements and the element interlocking can cause initial penetration and crossed edges. Therefore, nodes on the soil interface are modelled to be coincident with those of the tunnel interface to minimize the element inter-locking. The tunnel uses three elements across its thickness to facilitate a nonlinear stress distribution through the thickness. The tunnel is further refined with a gradual increase in element size in both axial and circumferential directions away from the incident blast. The size of the smallest element in the tunnel is 10.25 cm x 12.5 cm x 5.83 cm.

Journal of Performance of Constructed Facilities. Submitted September 20, 2013; accepted January 22, 2014; posted ahead of print January 25, 2014. doi:10.1061/(ASCE)CF.1943-5509.0000585

The spherical shape explosive is defined into the background mesh by using *INITIAL_ VOLUME_FRACTION_GEOMETRY, by specifying its radius and detonation point. The contact interface simulation between the soil and the tunnel surfaces is crucial to an accurate analysis of tunnel response. In LS-DYNA, *CONTACT_AUTOMATIC_SURFACE_ TO_SURFACE type contact algorithm permits separation, recontact and sliding of the two surfaces.

The translational displacements of symmetry boundaries XZ and YZ planes (Fig. 2) are constrained in their normal directions. Reflection of shock waves at the far-field can affect the accuracy of the numerical simulation. In LS-DYNA, non-reflecting boundary condition allows the shock wave to flow out through both Eulerian and Lagrangian meshes. The non-reflecting boundary condition is therefore applied to the infinite domain while the base is fixed in all directions to represent the bed rock.

The material models and relevant material properties for the air, soil, explosive and copper described in the section of Material Constitutive Models are employed in the model.

Three stage simulation

In order to minimise the computational cost, the numerical modelling technique relates to a time-ordered sequence of interrelated phases which describe the entire simulation. LS-DYNA's restart feature enables to break the entire simulation into three stages such as stress initialization, ALE/Lagrangian coupling and deletion of ALE background mesh.

Journal of Performance of Constructed Facilities. Submitted September 20, 2013; accepted January 22, 2014; posted ahead of print January 25, 2014. doi:10.1061/(ASCE)CF.1943-5509.0000585

Stress initialization

In geotechnical modelling, stress initialisation is essential to induce a steady state preload in the Lagrangian structure before applying a transient dynamic load such as blast. The simulation utilises time dependent mass damping option *DAMPING_GLOBAL in LS-DYNA to impose near-critical damping until the preload is established. The mass damping algorithm could be used in an explicit finite element code such as LS-DYNA to evaluate the initial geostatic stress of large underground structures. The model was preloaded quasi-statically with a ramp load function. This option was activated after first peak deformation cycle. For stability reasons, the analysis was conducted with a default time step SF of 0.90. Fig. 3 shows the Kinetic Energy (KE) vs. time plot during the stress initialization, where the KE converged to zero at 1500 ms.

Furthermore, three gauge points such as on tunnel crown, springline and invert of the tunnel cross section at midspan verify the initialization process by using vertical displacement vs. time plots as shown in Fig. 4.

ALE/Lagrangian coupling

Fig. 5 describes the background mesh insertion into the preloaded Lagrangian model. Activation of ALE/Lagrangian coupling (*CONSTRAINED_LAGRANGE_IN_SOLID) computes the penetration of the ALE meshes across the lagrangian structure during load transfer. Level of accuracy in ALE/Lagrangian coupling depends on an appropriate degree of refinement of ALE mesh inside the lagrangian parts. Smaller ALE mesh size increases computational time. Therefore, for adequate solution, at least 10 elements in the ALE mesh flow passage need to be nearly the same size as the lagrangian mesh.

Journal of Performance of Constructed Facilities. Submitted September 20, 2013; accepted January 22, 2014; posted ahead of print January 25, 2014. doi:10.1061/(ASCE)CF.1943-5509.0000585

The ALE/Lagrangian coupling phase is more expensive than the other two phases as it deals with FSI which is complex to solve analytically. However, the duration for the blast load transfer from ALE domain to Lagrangian parts is considerably small as evident from Fig. 6. It can be observed from the KE vs. time plot in this Figure that the KE of ALE background mesh is sufficiently reduced to zero in about 180 ms. In other words, ALE parts are only necessary for duration of the load transfer and are ineffective beyond that time (even if the analysis continues without removing them).

Deletion of ALE background mesh

LS-DYNA's restart features *DELETE_PART and *DELETE_FSI allow to remove the redundant ALE background mesh and ALE/Lagrangian coupling respectively. Deletion of redundant elements from the model reduces the computational time considerably. The simulation is continued with the remaining lagrangian structure until the copper tunnel response comes to rest.

Numerical Validation and Discussion

This section presents the results and discussion on the dynamic response of the copper tunnel during the last two phases: ALE/Lagrangian coupling and Deletion of ALE background mesh. After stress initialization, the explosion was initiated at 1500 ms. The simulation deals with an equivalent explosive weight of 888 kg TNT in a prototype model to represent De (De 2012)'s scaled-down model.

Shock wave propagation in soil

Fig. 7 describes the shock wave propagation through the soil while creating a crater. The shock wave travels in the soil in the form of hemispherical waves. The area of wave front

Journal of Performance of Constructed Facilities. Submitted September 20, 2013; accepted January 22, 2014; posted ahead of print January 25, 2014. doi:10.1061/(ASCE)CF.1943-5509.0000585

expands with the wave propagation. The wave front reached the tunnel surface after 7 ms of explosion as illustrated in Fig. 7.

Without the tunnel structure, a free field model as shown in Fig. 8, was considered to monitor the shock wave propagation in soil. Fig. 9 illustrates the arrangement of measuring gauges at 3 m spacing along two grid directions. Grid 1 is vertically below the explosive while Grid 2 is inclined by 450 to the ground surface. Gauges in Grid 1 are located in the central zone (Yang et al. 2010) to capture the intensity of shock wave which is mainly due to the compressive waves in the soil. Gauges in Grid 2 are located at the interface between the central and surface zones (Yang et al. 2010). Fig. 10 shows the peak pressure variation with respect to the equivalent scaled distance of $R/W^{1/3}$ to the explosive. The propagation and attenuation of the shock waves in soil are clearly demonstrated by the two plots in Grid 1 and Grid 2. By comparing readings in Grid 1 and Grid 2, it is evident that gauges in Grid 1 experienced slightly higher peak pressures than the corresponding gauges in Grid 2. This could be due to the fact that the corresponding gauges in Grid2 are shallower and located in the interface between the central and surface zones.

Empirical equations of the power law in the technical manual TM5-855-1 (Vicksburg 1986) can be used to estimate the peak pressure range. In order to derive equations for the type of soil considered in the simulation, the more appropriate soil properties of acoustic impedance (*pc*) and attenuation coefficient (*n*) are selected as 51.41 kPa/ms^{-1} and 2.625±0.125 (Vicksburg 1986) respectively, for a known seismic speed. The following two empirical equations are derived by substituting the upper and lower limits of n in the TM5-855-1 empirical equations for free field pressure. These two equations are plotted on a logarithmic

Journal of Performance of Constructed Facilities. Submitted September 20, 2013; accepted January 22, 2014; posted ahead of print January 25, 2014. doi:10.1061/(ASCE)CF.1943-5509.0000585

scale as two straight lines shown in Fig. 10. The slope of a straight line represents the attenuation coefficient.

$$P_0 = f \cdot 22 \cdot \left(\frac{R}{\sqrt[3]{W}} \right)^{-2.75} ; \quad n = 2.75 \qquad \text{Eq. 14}$$

$$P_0 = f \cdot 27 \cdot \left(\frac{R}{\sqrt[3]{W}} \right)^{-2.50} ; \quad n = 2.50 \qquad \text{Eq. 15}$$

where P_0 is the peak pressure in Mpa, f is the coupling factor which has a recommended constant value of $f = 0.14$ for explosion in air, R is the distance to the explosive in m, and W is the explosive weight in kg.

Gauge readings along Grid 1 agreed reasonably well with the estimated peak pressure values from Eq. 15. Shallower depth readings along Grid 2 slightly deviated from both straight lines, but they fell into the straight lines as the depth increased beyond the scale distance 1.60. This discrepancy may result from the limitation of power law for a certain distance range (Yankelevsky et al. 2011). According to Yankelevsky et al. (Yankelevsky et al. 2011) some types of soils may not be represented by a linear relationship on a logarithmic scale, but need to be described by either bi-linear or tri-linear relationships.

Response of copper tunnel in dry sand

The tunnel started to respond to the blast when the shock wave hit the tunnel and the response continued until the shock wave completely attenuated in the soil. Fig. 11 shows the time history of kinetic energy (KE) of the tunnel response after the explosion. The tunnel response commenced at t = 1507 ms by imparting inertia load to the tunnel from the surrounding soil

Journal of Performance of Constructed Facilities. Submitted September 20, 2013; accepted January 22, 2014; posted ahead of print January 25, 2014. doi:10.1061/(ASCE)CF.1943-5509.0000585

and the response reached its peak within 4.5 ms. The tunnel dissipated 90% of its KE within 23 ms of initial response period.

The process of the pressure wave propagation through the tunnel is presented in Fig. 12 at different time intervals of the tunnel response. While the pressure wave travelled along both the longitudinal and the circumferential directions of the tunnel, positive and negative phases of pressure contours changed with time.

Two gauges Gauge 1 and Gauge 2 were introduced along the surface of tunnel crown to record the axial and circumferential strains in the numerical analysis. Gauge 1 was located directly below the explosive center on the tunnel surface while Gauge 2 was placed 10.6 m away from Gauge 1 as shown in Fig. 13. Gauge 3 was placed on the springline of the midspan to monitor the circumferential strain in the numerical analysis.

Studies were performed initially without considering the mesh alignment on the curved contact interface between the soil and tunnel. Interlocking due to peaks and valleys on the interface governed the tunnel response rather than the frictional forces. Interlocking of contact surfaces constrained the tunnel response in circumferential direction as in a perfectly bonded interface. Results reported are not presented here, but the important finding has been used in this numerical simulation to avoid the interlocking of elements.

Fig. 14 shows the time histories of the axial and circumferential strains at the above mentioned Gauge positions. Both plots show that the tunnel response decreases with increase in distance from the explosive, in both axial and circumferential directions, as the intensity of shock wave decays along the tunnel. The plots further indicate that all deformations at gauge

Journal of Performance of Constructed Facilities. Submitted September 20, 2013; accepted January 22, 2014; posted ahead of print January 25, 2014. doi:10.1061/(ASCE)CF.1943-5509.0000585

points travelled through a peak response cycle over a period of 23 ms (1507 ms-1530 ms). In this period, the tunnel lost about 90 % of peak KE. Therefore, it would be appropriate to say that, this might be the critical period of tunnel response.

Furthermore, it is observed in Fig. 14(a) that most of the axial deformation is recoverable although the response continued with a noticeable fluctuation in axial strain. It is also evident that the circumferential deformation, obtained from Gauges 2 & 3, recovered as shown in Fig. 14(b). However, from the circumferential residual strain at Gauge 1, it is clear that the tunnel suffered permanent deformation due to the surface explosion. This state of strains is reasonable because the tunnel has an infinite surface area in the longitudinal direction which constrained its movement due to the grip in the contact surface between the tunnel and the soil. In the transverse direction, excessive compressive stress from the blast load changed its deformation mode to a horizontal ovalisation as shown in Fig. 15. The deformation mode depends on degree of flexibility of the tunnel structure. Due to this, some researchers (Gui and Chien 2006; Shin et al. 2011) have treated the tunnel response using two dimensional plane-strain analysis by omitting the axial deformation.

The higher value of the circumferential strain at Gauges 1 compared to that at Gauge 3 highlight that the upper part of tunnel above the springline is vulnerable to the explosion. This suggests possible blast mitigation of the tunnel by providing a protective cover on the top half of the tunnel and if tension is evident providing appropriate tensile reinforcement (where necessary) for non-metallic tunnels. Fig. 16(a) demonstrates how the axial strain varies along the surface of the tunnel crown when Gauge 1 responded to the peak axial strain (deformation) at 1513 ms. During this time, as illustrated in Fig. 12(c), the shock wave front

Journal of Performance of Constructed Facilities. Submitted September 20, 2013; accepted January 22, 2014; posted ahead of print January 25, 2014. doi:10.1061/(ASCE)CF.1943-5509.0000585

was slightly less than 5.0 m away from the midspan of the tunnel. These two figures show that Gauge 1 exhibited the peak axial tensile strain after the shock wave travelled through the target. Propagating shock wave compressed the portion of the tunnel ahead of the shock wave. Furthermore, it displayed a decrease of the axial compressive strain followed by a peak axial compressive strain at 5.0 m from the midspan. The compressive zone extended over 5.0 m, beyond which there were no significant effect in axial strain. Similarly, Fig. 16(b) describes the distribution of the circumferential strain along the arc distance away from the top of the tunnel mid-span when the same target was subjected to peak deformation at 1510 ms. In this time, propagating shock waves were within an angle of 45^0 from the crown, which can be seen from Fig. 12(b). The circumferential tensile strain rapidly decreased to a small magnitude at a position of 32.5^0. Due to the globalized vertical in-plane response, the circumferential strain was in tension ahead of the shock wave and it extended even below the springline. Although most surfaces were in tension, the region close to the invert level was slightly in compression.

Comparisons of the tunnel response with available experimental results of a centrifuge test (De 2012; De and Zimmie 2006) were carried out. Fig. 17 compares the numerical strain history at Gauge 2 with that from the centrifuge test (De and Zimmie 2006). The proximity of the two curves, with closely matching peaks, indicates a reasonably good correlation between the numerical and the experimental results and provides adequate confidence in the present modelling techniques. Furthermore, in Fig. 18, magnitudes of peak axial and circumferential strains at Gauge 1 and Gauge3 respectively, are plotted against the equivalent scaled distance by varying the explosive weight and the soil cover. These strains obtained from the LS-DYNA analysis are compared with those from the centrifuge test (De 2012) (measured for a

Journal of Performance of Constructed Facilities. Submitted September 20, 2013; accepted January 22, 2014; posted ahead of print January 25, 2014. doi:10.1061/(ASCE)CF.1943-5509.0000585

specific value of the scaled distance). There is a small discrepancy in the axial strains in Fig. 18(a), as was also observed in the numerical simulations reported in (De 2012). This could be due to the uncertainties in the end condition of the pipe and the limitations in its movement in the experiment. A real buried tunnel in a soil medium has no movement restrictions, but the experimental model had restrictions from the four sides of the test-bucket (box in Fig. 1) containing the soil. These constrained boundaries may restrict the combined motion of soil and the pipe.

The circumferential strains at Gauge 3 obtained from the numerical simulations were compared with the experimental results at the two points CS1 & CS2 as illustrated in Fig. 18(b). These two points are symmetrically located on either side of the springline at the midspan in the experimental setup. The comparisons show that the numerical best-fit line lies between the experimental values at CS1 & CS2. Under symmetric condition of blast loading and the symmetric locations of gauges CS1 & CS2, the peak strains measured in the experiment should be the same at both locations. However, this was not the case and a variation of 280 microstrain was noted. This lack of symmetry and variation in results at CS1 & CS2 could be due to possible movement of the explosive from its initial position inside the test-bucket before the blast occurred or due to a rotation of the copper pipe about its axis during the placement and sand filling into the test-bucket. In centrifuge tests, controlling measures are very difficult to implement, particularly, in blast loading.

These observations of different circumferential strains at two initially symmetric locations demonstrate the possible movement of the tunnel or explosive during testing and resulting in the actual value of the peak axial strain (at the top of the tunnel at midspan) to be more than

Journal of Performance of Constructed Facilities. Submitted September 20, 2013; accepted January 22, 2014; posted ahead of print January 25, 2014. doi:10.1061/(ASCE)CF.1943-5509.0000585

the value measured in the experiment. This justifies the higher value of the numerical axial strain compared to this measured value.

Tunnel Response in Saturated Sand

This study further investigated the response of the tunnel buried in saturated sand using the same modelling techniques described in the earlier section. The main parameters for the saturated sand were evaluated based on the section of 'Soil' and values suggested by Lee (2006). Table 6 describes the soil parameters.

As shown in Fig. 19, the shock wave front reached the tunnel crown after 4 ms of the explosion whereas it occurred in dry sand after 7 ms of the explosion. It is due to the fact that the blast induced shock waves are rich in primary wave content and are faster in saturated sand than in the dry sand. It is also evident that the pressures are significantly larger in magnitude than those in dry sand (Fig. 7). As a result, it triggered the early response as well larger impact on the tunnel response.

Fig. 20 illustrates the axial and circumferential strain histories at the tunnel surface and it can be seen that the axial and circumferential deformations are in general larger in the saturated sand than in the dry sand (Fig. 14). Furthermore, comparisons of circumferential strains in both sands at Gauge 1 show that the residual strain of the tunnel in the saturated sand is 54% higher than that in dry sand due to the liquefaction of the soil in the vicinity of the tunnel crown caused by the blast. The blast induced liquefaction increased the pore-water pressure which could exert higher pressure on the tunnel. Fig. 20 also shows that Gauge 1 in saturated sand shows a larger irrecoverable axial strain compared to that in dry sand. Axial

Journal of Performance of Constructed Facilities. Submitted September 20, 2013; accepted January 22, 2014; posted ahead of print January 25, 2014. doi:10.1061/(ASCE)CF.1943-5509.0000585

deformations at Gauge 2 are moderately higher for the saturated sand, but these axial deformations seem to have recovered in both sands. Peak circumferential deformations at Gauge 3 for saturated sand are also higher than those in dry sand, but these deformations also largely recovered. Comparison of blast response of the tunnel in dry and saturated sands reveals that the response in the vicinity of the explosive is more severe in saturated sand than that in dry sand.

Conclusion

This paper used finite element techniques to investigate the performance of buried tunnels subjected to surface blasts incorporating fully coupled Fluid Structure Interaction (FSI) and appropriate material models which simulate strain rate effects. The combination of FSI and the restart feature in LS-DYNA effectively handled the entire simulation by adding and deleting elements in representing different physical processes of stress initialization and blast analysis. Validated modelling techniques using existing experimental results were used to treat the blast induced shock wave propagation and tunnel response in dry and saturated sands. This study used '*MAT_FHWA_SOIL' soil model which is relatively simple and it simulates pore-water, strain rate effect and strain softening in soil. The main findings of this study can be summarised as follows:

- The tunnel buried in saturated sand responded to the blast loading earlier than that in dry sand.
- The axial and circumferential deformations decrease with increasing distance from the explosive in both sands, as expected.
- The circumferential strain histories indicate that the upper part of tunnel above the spring-line is more vulnerable to the explosion than the lower part. This will suggest

Journal of Performance of Constructed Facilities. Submitted September 20, 2013; accepted January 22, 2014; posted ahead of print January 25, 2014. doi:10.1061/(ASCE)CF.1943-5509.0000585

the provision of a protective layer at the top half of the tunnel for blast mitigation. In addition, for tunnels made of non-metal materials (such as concrete) tensile failure needs to be avoided, perhaps by provision of appropriate reinforcement.

- In dry sand, the tunnel recovered from most of the axial deformations while it resulted with a permanent deformation at the top of the mid-span in the circumferential direction. However, in saturated sand, the tunnel suffered irrecoverable deformation in both axial and circumferential directions. The response of the tunnel buried in the saturated sand is more severe for a given blast event. These results demonstrate the detrimental effects of pore water on the blast response of buried tunnels.
- The validated numerical results provide confidence in the modelling techniques used in this study and allow developing rational procedures for predicting the blast response of buried cylindrical structures in dry and saturated sands.

NOTATIONS

The following symbols are used in this paper:

R	=	tunnel radius;
ρ	=	density;
G_s	=	specific gravity
G	=	shear modulus;
K	=	bulk modulus;
c	=	sound speed;
V_P	=	velocity of primary wave;
V_S	=	velocity of shear wave;
υ	=	Poisson's ratio;
n	=	soil porosity;
S	=	degree of saturation;
B	=	Skempton pore-water pressure parameter;
u	=	pore-water pressure;
ε_v	=	volumetric compression strain; and
D_2	=	a function of Skempton's pore-water pressure.

Journal of Performance of Constructed Facilities. Submitted September 20, 2013; accepted January 22, 2014; posted ahead of print January 25, 2014. doi:10.1061/(ASCE)CF.1943-5509.0000585

References

Abbo, A. J., and Sloan, S. W. (1995). "A smooth hyperbolic approximation to the Mohr-Coulomb yield criterion." *Computers & Structures*, 54(3), 427-441.

Ambrosini, D., Luccioni, B., and Danesi, R. (2003). "Influence of the soil properties on craters produced by explosions on the soil surface." *Computational Mechanics*, 571-590.

Arulmoli, K., Project, V., Corporation, E. T., and Foundation, N. S. (1992). *VELACS Verification of Liquefaction Analyses by Centrifuge Studies Laboratory Testing Program: Soil Data Report*, Earth Technology Corporation.

Barsotti, M. A., Puryear, J. M. H., Stevens, D. J., Alberson, R. M., and McMohon, P. (2012). "Modeling Mine Blast with SPH." *12th International LS-DYNA Users Conference,*Dearborn, Michigan.

Davies, M. C. R. "Dynamic Soil Structure Interaction Resulting from Blast Loading." *Proc., Centrifuge 94. Rotterdam:Balkema*, 319-324.

De, A. (2012). "Numerical simulation of surface explosions over dry, cohesionless soil." *Computers and Geotechnics*, 43(0), 72-79.

De, A., Morgante, A. N., and Zimmie, T. F. (2013). "Mitigation of Blast Effects on Underground Structure Using Compressible Porous Foam Barriers." *Poromechanics V*, 971-980.

De, A., and Zimmie, T. F. "Modeling of Surface Blast Effects on Underground Structures." *Proc., GeoCongress, ASCE.*

De, A., and Zimmie, T. F. (2007). "Centrifuge modeling of Surface Blast Effects on Underground Structures." *Geotechnical Testing Journal*, 30, 427-431.

Feldgun, V. R., Kochetkov, A. V., Karinski, Y. S., and Yankelevsky, D. Z. (2008). "Internal blast loading in a buried lined tunnel " *International Journal of Impact Engineering* 35, 172 - 183.

Gui, M., and Chien, M. (2006). "Blast-resistant Analysis for a Tunnel Passing Beneath Taipei Shongsan Airport–a Parametric Study." *Geotechnical and Geological Engineering*, 24(2), 227-248.

Higgins, W., Chakraborty, T., and Basu, D. (2012). "A high strain-rate constitutive model for sand and its application in finite-element analysis of tunnels subjected to blast." *International Journal for Numerical and Analytical Methods in Geomechanics (2012).*

Higgins, W. T. (2011). "Development of a high strain-rate constitutive model for sands and its application in finite element analysis of tunnels subjected to blast." University of Connecticut, Storrs, Connecticut, USA.

Journal of Performance of Constructed Facilities. Submitted September 20, 2013; accepted January 22, 2014; posted ahead of print January 25, 2014. doi:10.1061/(ASCE)CF.1943-5509.0000585

Jayasinghe, L. B., Thambiratnam, D. P., Perera, N., and Jayasooriya, J. H. A. R. (2013). "Computer simulation of underground blast response of pile in saturated soil." *Computers & Structures*, 120(0), 86 - 95.

Koneshwaran, S., Thambiratnam, D. P., and Gallage, C. "Response of a Buried Tunnel to Surface Blast using Different Numerical Techniques." *Proc., Proceedings of the Fourteenth International Conference on Civil, Structural and Environmental Engineering Computing*, Civil-Comp Press, Stirlingshire, UK.

Kramer (1996). *Geotechnical Earthquake Engineering*, Pearson Education.

Kutter, B. L., O'Leary, L. M., and Thompson, P. Y. (1988). "Gravity-Scaled Tests on Blast-Induced Soil-Structure Interaction." *Journal of Geotechnical Engineering,*, 114, 431-447.

Laine, L., and Sandvik, A. (2001). "Derivation of Mechanical properties for sand." *Proceedings of the 4th Asia-Pacific Conference on Shock and Impact Loads on Structures, CI-Premier PTE LTD, Singapore*, 361-368.

Lee, W. Y. (2006). "Numerical modeling of blast-induced liquefaction." Department of Civil and Environmental Engineering, Brigham Young University.

Lewis, B. A. (2004). "Manual for LS-DYNA Soil Material Model 147."Federal Highway Administration, McLEAN, VA.

Liu, H. (2009). "Dynamic Analysis of Subway Structures Under Blast Loading." *Geotechnical and Geological Engineering*, 27(6), 699-711.

Liu, H. (2012). "Soil-Structure Interaction and Failure of Cast-Iron Subway Tunnels Subjected to Medium Internal Blast Loading." *Journal of Performance of Constructed Facilities*, Vol. 26, 691-701.

LSTC. (2007). "LS-DYNA Keyword User's Manual v971, Livermore Software Technology Corporation(LSTC)." *California, USA*.

Matuska, D. A. (1984). "HULL Users' Manual." DTIC Document.

Monaghan, J. J. (2000). "SPH without a Tensile Instability." *Journal of Computational Physics*, 159(2), 290 - 311.

Naesgaard, E., Byrne, P. M., and Wijewickreme, D. (2007). "Is P-wave velocity an indicator of saturation in sand with viscous pore fluid?" *International Journal of Geomechanics*, 7(6), 437-443.

Olarewaju, A. J. (2012 (a)). "Study on the Impact of Varying Degrees of Underground Accidental Explosions on Underground Pipes by Simulation." *Earth Science Research, Published by Canadian Centre of Science and Education*, Vol.1, No. 2, 189-199.

Olarewaju, A. J. (2012 (b)). "Effect of Loose Sand and Dense Sand on the Response of Underground Empty Pipes due to Accidental Explosions." *Electronic Journal of Geotechnical Engineering (EJGE)*, Vol. 17 Bundle G, 879-891.

Olarewaju, A. J. (2013). "Prediction and Assessment of Loads from Various Accidental Explosions for Simulating the Response of Underground Structures using Finite Element Method." *Electronic Journal of Geotechnical Engineering (EJGE)*, Vol. 18 Bundle B, 375-396.

Peroni, M., Peroni, L., and Dallocchio, A. (2009). "Thermo-mechanical model identification of a strengthened copper with an inverse method." *DYMAT 2009-9th International Conference on the Mechanical and Physical Behaviour of Materials under Dynamic Loading*, 1367-1373.

Saleh, M., and Edwards, L. (2011). "Application of a soil model in the numerical analysis of landmine interaction with protective structures " *26th International symposium on blastics MIAMI*FL.

Shin, J. H., Moon, H. G., and Chae , S. E. (2011). "Effect of blast-induced vibration on existing tunnels in soft rocks." *Tunnelling and Underground Space Technology*, 26(1), 51-61.

Vicksburg (1986). "US Army Engineers Waterways Experimental Stations, (1986) Fundamental of Protection Design for Conventional Weapons, TM 5-855-1.".

Wang, Z., Lu, Y., Hao, H., and Chong, K. (2005). "A full coupled numerical analysis approach for buried structures subjected to subsurface blast." *Computers & Structures*, 83(4-5), 339-356.

Whittaker, J. P. (1987). "Centrifugal and numerical modeling of buried structures. Volume 3. A centrifuge study of the behavior of buried conduits under airblast loads. Final report." Colorado Univ., Boulder (USA). Dept. of Civil, Environmental, and Architectural Engineering.

Yang, Y., Xie, X., and Wang, R. (2010). "Numerical simulation of dynamic response of operating metro tunnel induced by ground explosion." *Journal of Rock Mechanics and Geotechnical Engineering*, 373-384.

Yankelevsky, D. Z., Karinski, Y. S., and Feldgun, V. R. (2011). "Re-examination of the shock wave's peak pressure attenuation in soils." *International Journal of Impact Engineering* 38(11), 864 - 881.

Journal of Performance of Constructed Facilities. Submitted September 20, 2013; accepted January 22, 2014; posted ahead of print January 25, 2014. doi:10.1061/(ASCE)CF.1943-5509.0000585

Table 1: Material properties for air (Yang et al. 2010)

ρ (g/cm^3)	C_0	C_1	C_2	C_3	C_4	C_5	C_6	E_0 (kJ/m^3)
1.29	0	0	0	0	0.4	0.4	0	0.25

Journal of Performance of Constructed Facilities. Submitted September 20, 2013; accepted January 22, 2014; posted ahead of print January 25, 2014. doi:10.1061/(ASCE)CF.1943-5509.0000585

Table 2: Material properties for TNT explosive) (Wang et al. 2005)

ρ (g/cm^3)	v_D (m/s)	P_{CJ} (GPa)	A (GPa)	B (GPa)	R_1	R_2	ω	V	E_0 (kJ/m^3)
1.630	6930	21	373.77	3.747	4.15	0.90	0.35	1	6.0e+06

Journal of Performance of Constructed Facilities. Submitted September 20, 2013; accepted January 22, 2014; posted ahead of print January 25, 2014. doi:10.1061/(ASCE)CF.1943-5509.0000585

Table 3: Material properties for copper

ρ (g/cm^3)	E (GPa)	υ	σ_y (MPa)	E_{tan} (MPa)	β	C (s^{-1})	P
8.93	117	0.35	400	100	0	1.346e+06	5.286

Journal of Performance of Constructed Facilities. Submitted September 20, 2013; accepted January 22, 2014; posted ahead of print January 25, 2014. doi:10.1061/(ASCE)CF.1943-5509.0000585

Table 4: Scaling law (Kramer 1996)

Type of event	Parameter	Model dimension / Prototype dimension
All events	Stress	1
	Strain	1
	Length	1/N
	Mass	$1/N^3$
	Density	1
	Force	$1/N^2$
	Gravity	N
Dynamic events	Time	1/N
	Acceleration	N
	Strain rate	N
Diffusion events	Time	$1/N^2$
	Strain rate	N^2

Journal of Performance of Constructed Facilities. Submitted September 20, 2013; accepted January 22, 2014; posted ahead of print January 25, 2014. doi:10.1061/(ASCE)CF.1943-5509.0000585

Table 5: Conversion to prototype model (De 2012)

Parameters	Scaled model dimension	Prototype model dimension
Copper tunnel diameter	76 mm	5.32 m
Copper tunnel thickness	2.5 mm	175 mm
Explosive weight of TNT	2.6 g	888 kg

Journal of Performance of Constructed Facilities. Submitted September 20, 2013; accepted January 22, 2014; posted ahead of print January 25, 2014. doi:10.1061/(ASCE)CF.1943-5509.0000585

Table 6: Material properties for saturated sand

ρ_{sat} (g/cm^3)	G_s	G_{sat} (Mpa)	K_{sat} (Mpa)	Moisture content (%)
1.84	2.67	56.0	3278.7	37.3

Journal of Performance of Constructed Facilities. Submitted September 20, 2013; accepted January 22, 2014; posted ahead of print January 25, 2014. doi:10.1061/(ASCE)CF.1943-5509.0000585

List of Figure Captions:

Fig. 1. Setup of experimental model and explosive (All dimensions are in prototype scale)

Fig. 2. A quarter symmetrical prototype model (Lagrangian structure)

Fig. 3. Kinetic energy vs. time during the initialization

Fig. 4. Displacement vs. time for three gauges

Fig. 5. Insertion of ALE background mesh into Lagrangian structure

Fig. 6. Kinetic energy vs. time plot of ALE background mesh

Fig. 7. Propagation of shock wave in dry sand

Fig. 8. Free field model for wave propagation study

Fig. 9. Arrangement of measuring gauge points

Fig. 10. Comparison of peak pressure distributions along Grid 1 and Grid 2

Fig. 11. Kinetic energy vs. time plot for tunnel

Fig. 12. Pressure wave propagation through the tunnel

Fig. 12(a). t = 1507 ms

Fig. 12(b). t = 1510 ms

Fig. 12(c). t = 1513 ms

Fig. 12(d). t = 1520 ms

Fig. 12(e). t = 1525 ms

Fig. 12(f). t = 1530 ms

Journal of Performance of Constructed Facilities. Submitted September 20, 2013; accepted January 22, 2014; posted ahead of print January 25, 2014. doi:10.1061/(ASCE)CF.1943-5509.0000585

Journal of Performance of Constructed Facilities. Submitted September 20, 2013; accepted January 22, 2014;
posted ahead of print January 25, 2014. doi:10.1061/(ASCE)CF.1943-5509.0000585

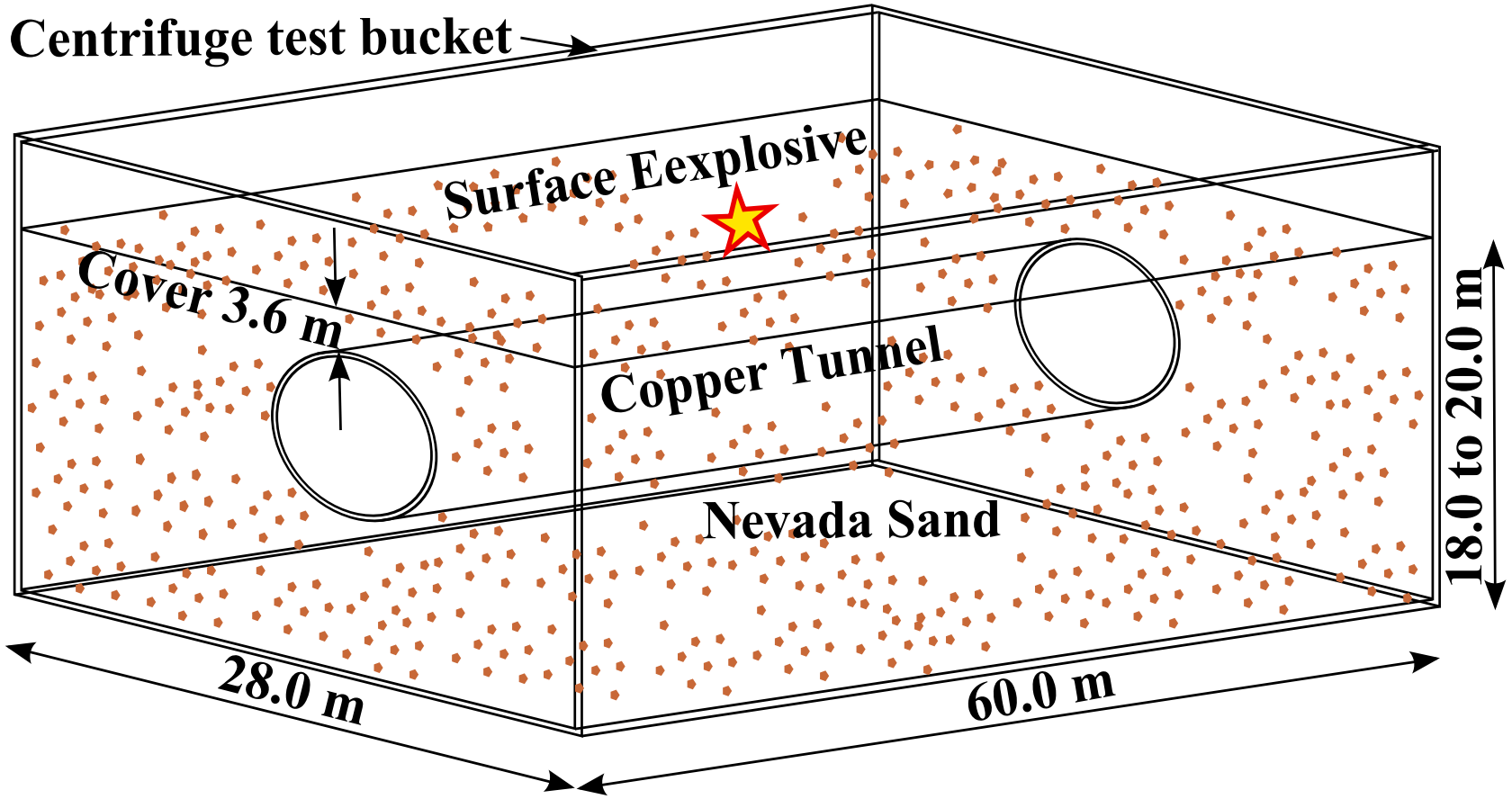

Journal of Performance of Constructed Facilities. Submitted September 20, 2013; accepted January 22, 2014;
posted ahead of print January 25, 2014. doi:10.1061/(ASCE)CF.1943-5509.0000585

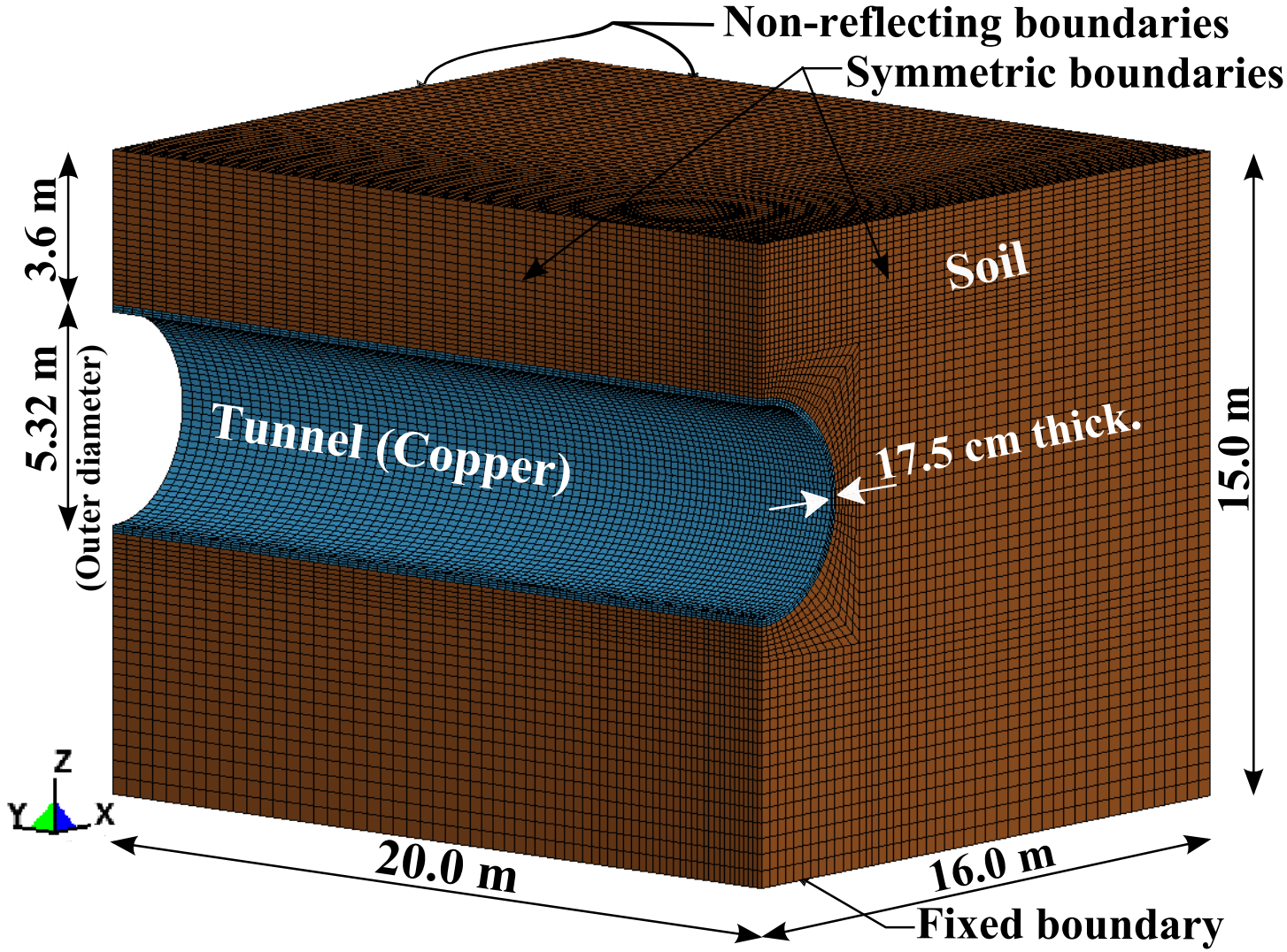

Journal of Performance of Constructed Facilities. Submitted September 20, 2013; accepted January 22, 2014;
posted ahead of print January 25, 2014. doi:10.1061/(ASCE)CF.1943-5509.0000585

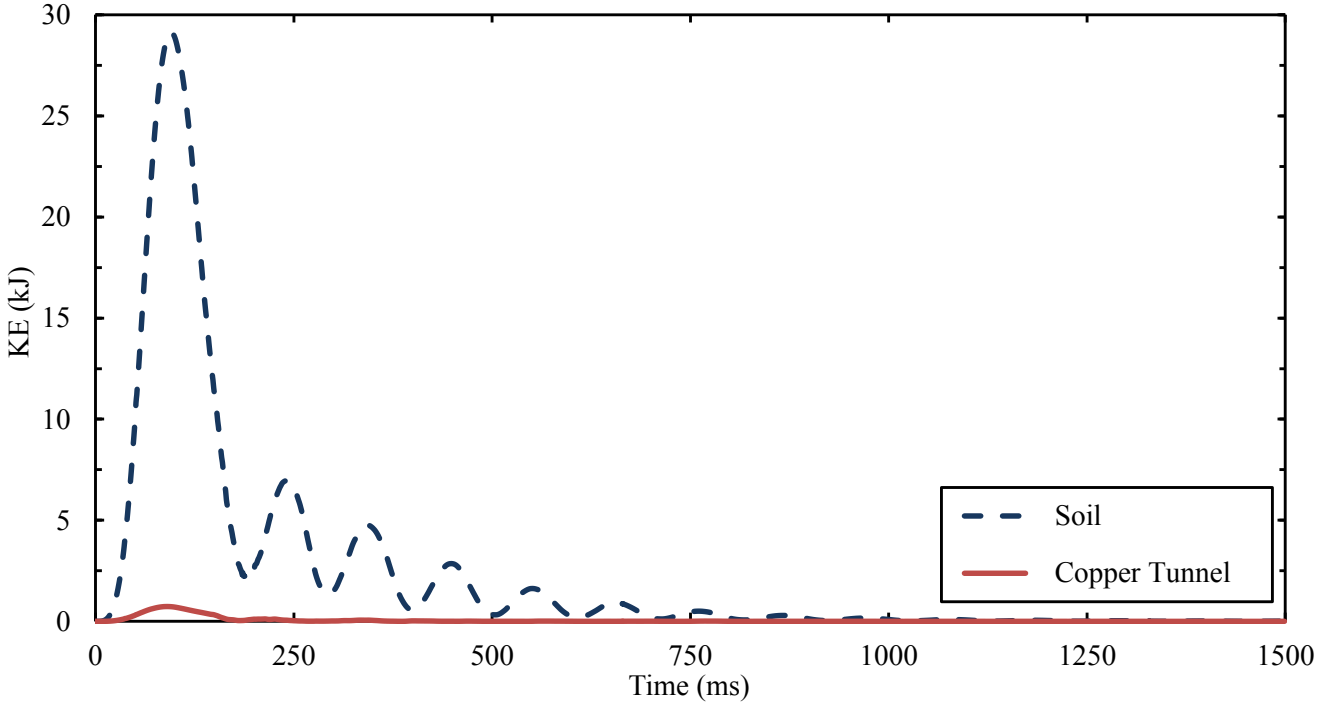

Journal of Performance of Constructed Facilities. Submitted September 20, 2013; accepted January 22, 2014;
posted ahead of print January 25, 2014. doi:10.1061/(ASCE)CF.1943-5509.0000585

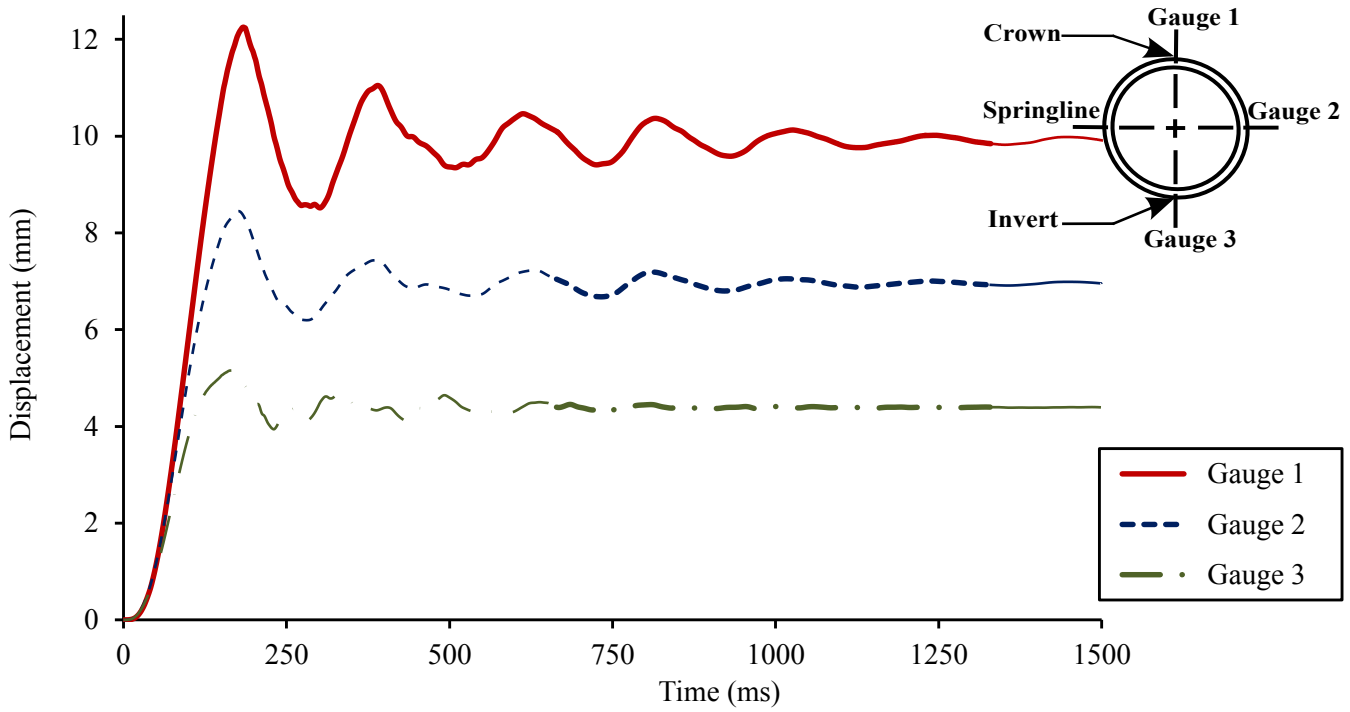

Journal of Performance of Constructed Facilities. Submitted September 20, 2013; accepted January 22, 2014;
posted ahead of print January 25, 2014. doi:10.1061/(ASCE)CF.1943-5509.0000585

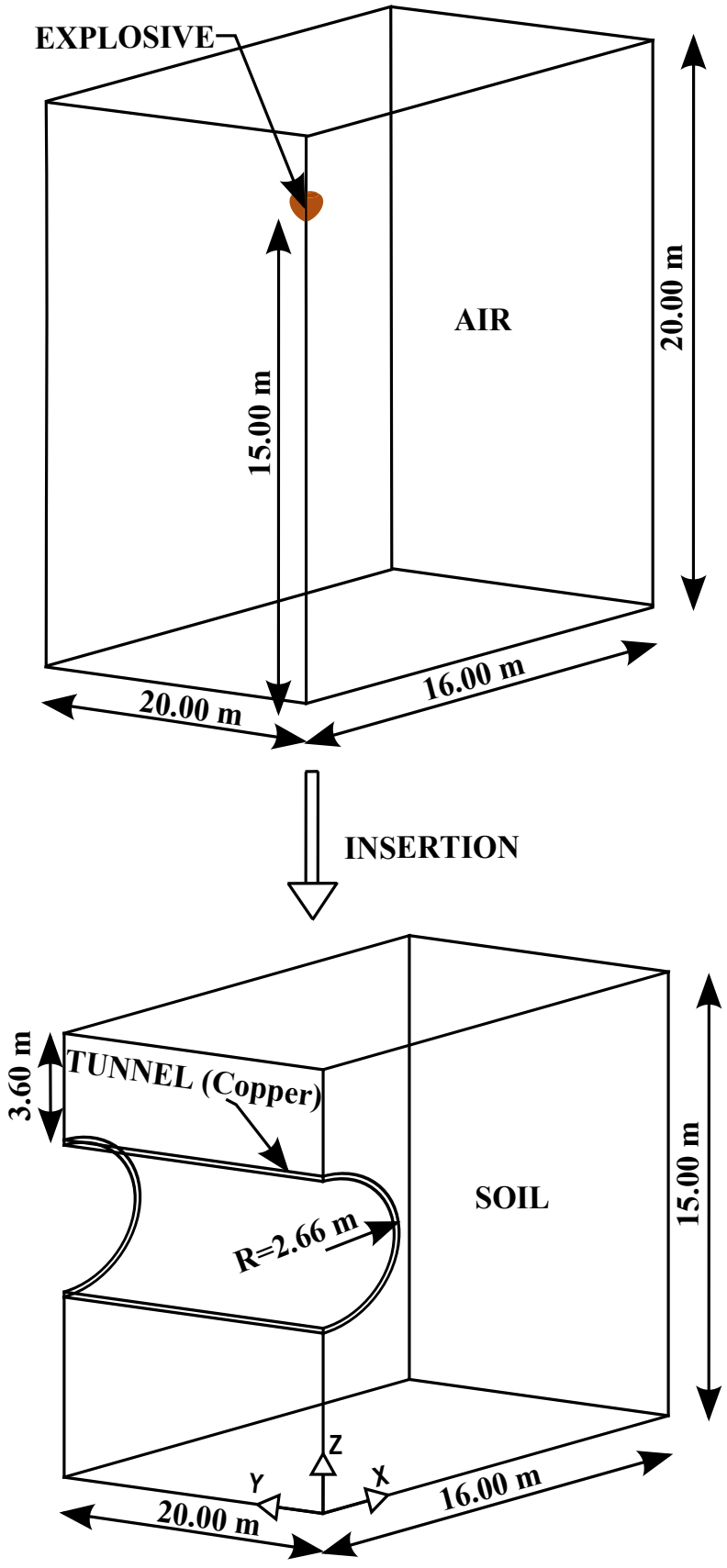

Journal of Performance of Constructed Facilities. Submitted September 20, 2013; accepted January 22, 2014;
posted ahead of print January 25, 2014. doi:10.1061/(ASCE)CF.1943-5509.0000585

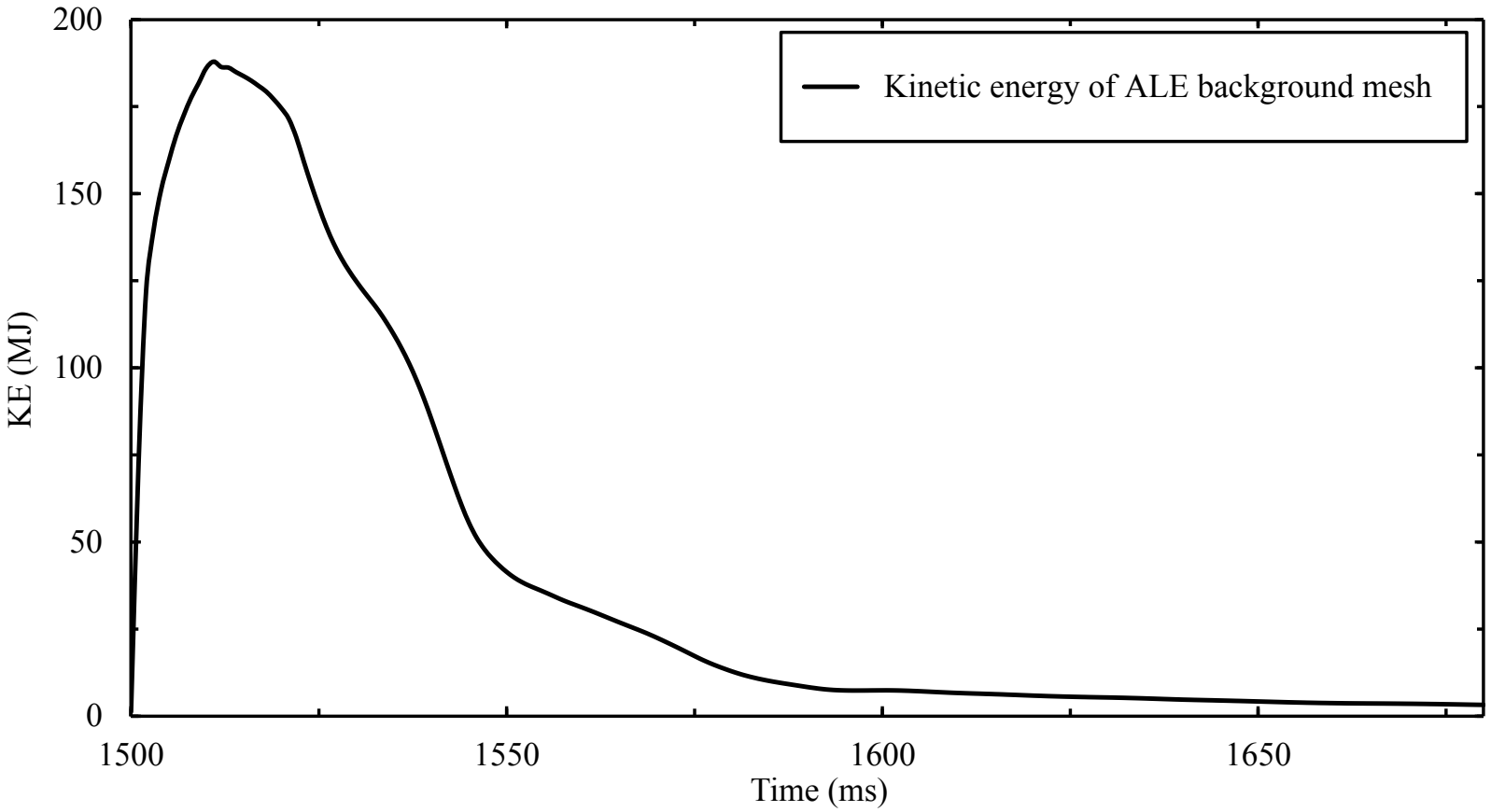

Journal of Performance of Constructed Facilities. Submitted September 20, 2013; accepted January 22, 2014;
posted ahead of print January 25, 2014. doi:10.1061/(ASCE)CF.1943-5509.0000585

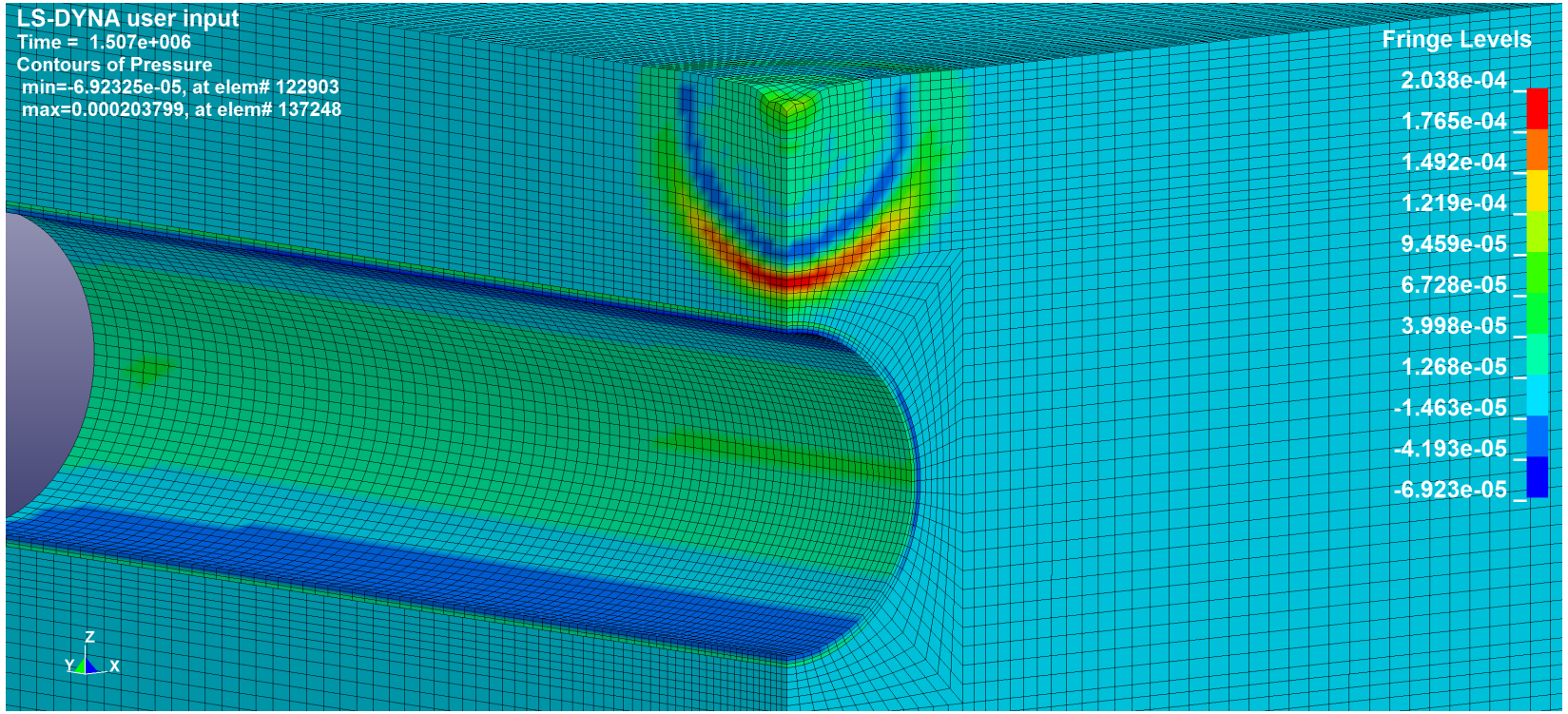

Journal of Performance of Constructed Facilities. Submitted September 20, 2013; accepted January 22, 2014;
posted ahead of print January 25, 2014. doi:10.1061/(ASCE)CF.1943-5509.0000585

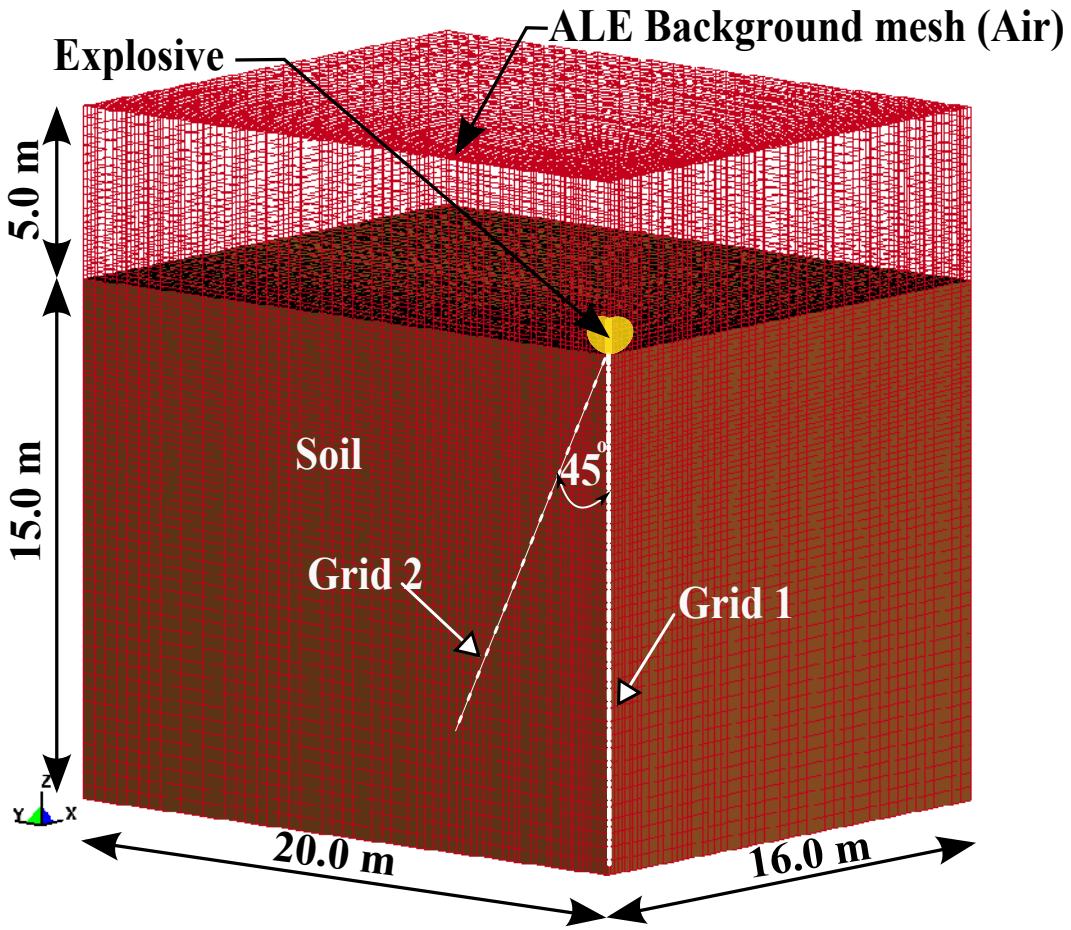

Journal of Performance of Constructed Facilities. Submitted September 20, 2013; accepted January 22, 2014;
posted ahead of print January 25, 2014. doi:10.1061/(ASCE)CF.1943-5509.0000585

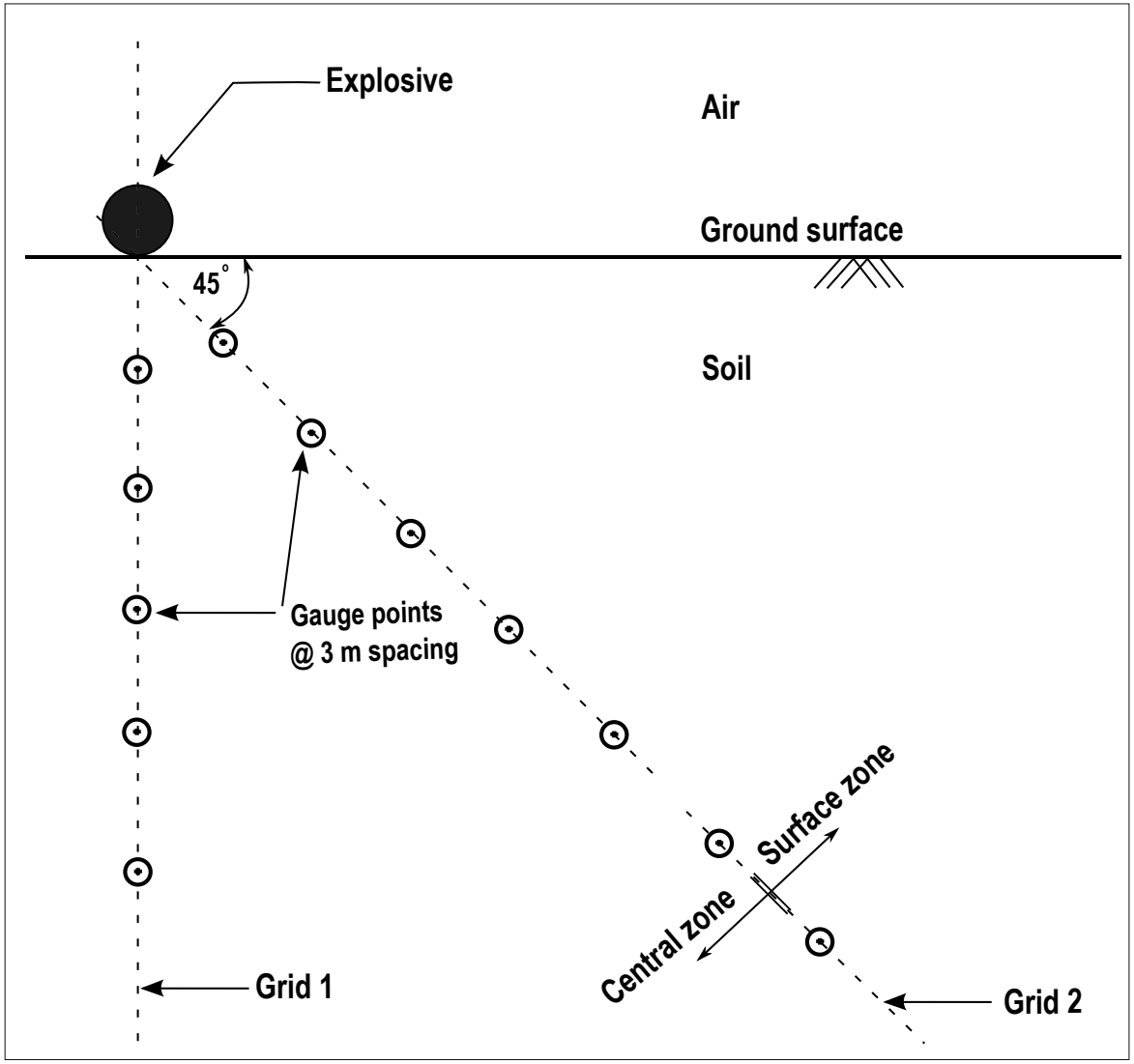

Journal of Performance of Constructed Facilities. Submitted September 20, 2013; accepted January 22, 2014;
posted ahead of print January 25, 2014. doi:10.1061/(ASCE)CF.1943-5509.0000585

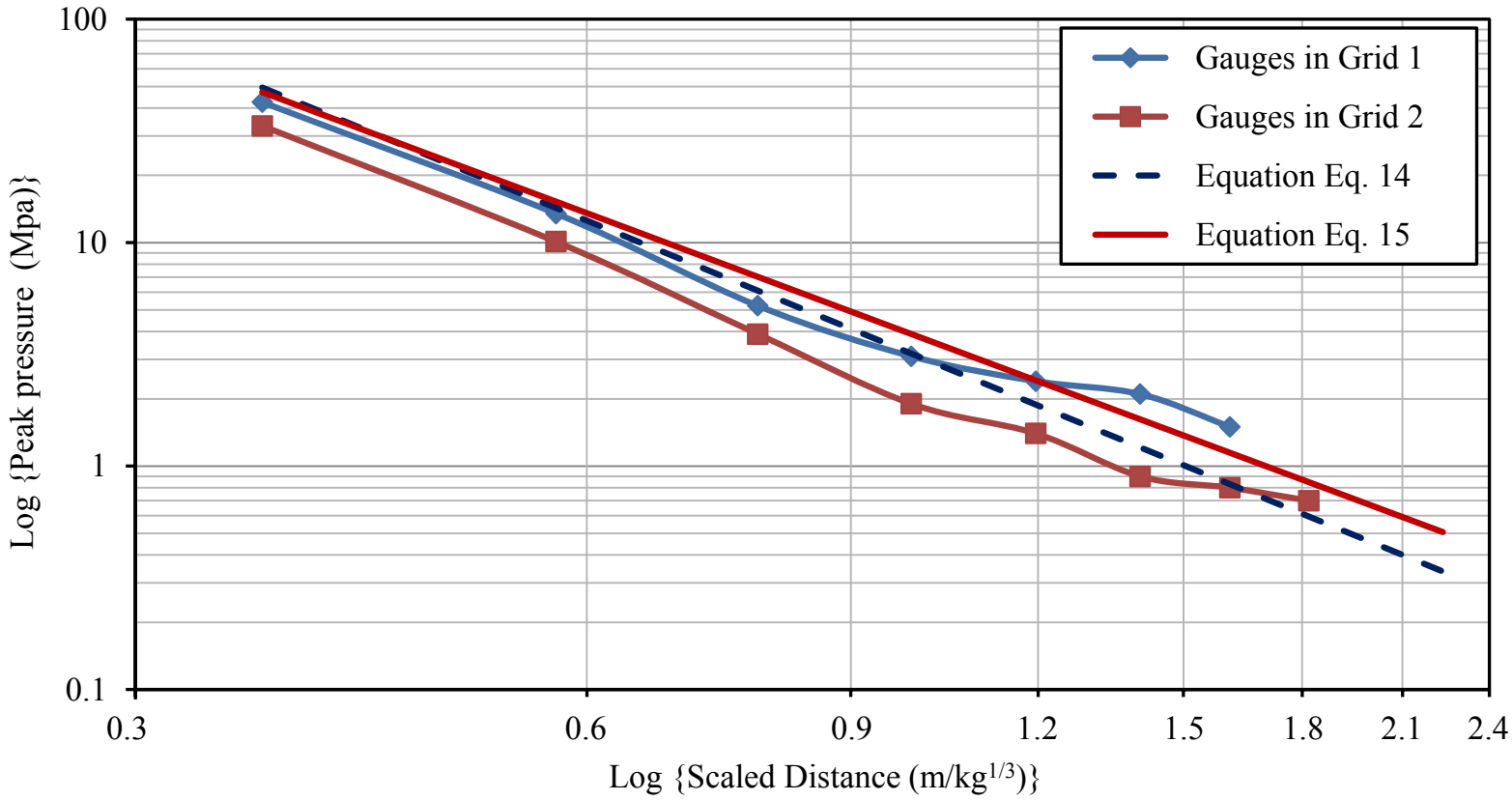

Journal of Performance of Constructed Facilities. Submitted September 20, 2013; accepted January 22, 2014;
posted ahead of print January 25, 2014. doi:10.1061/(ASCE)CF.1943-5509.0000585

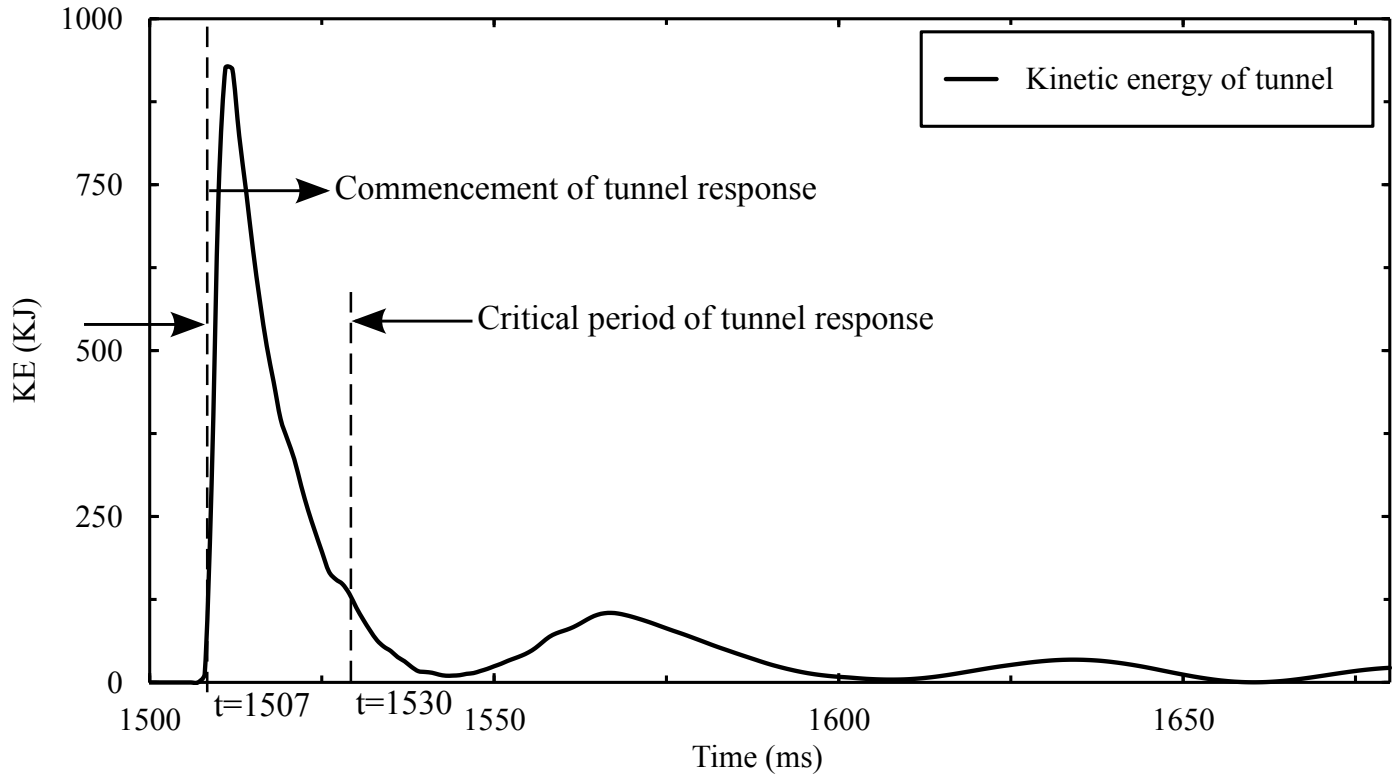

Fig 12(a).pdf

Journal of Performance of Constructed Facilities. Submitted September 20, 2013; accepted January 22, 2014;
posted ahead of print January 25, 2014. doi:10.1061/(ASCE)CF.1943-5509.0000585

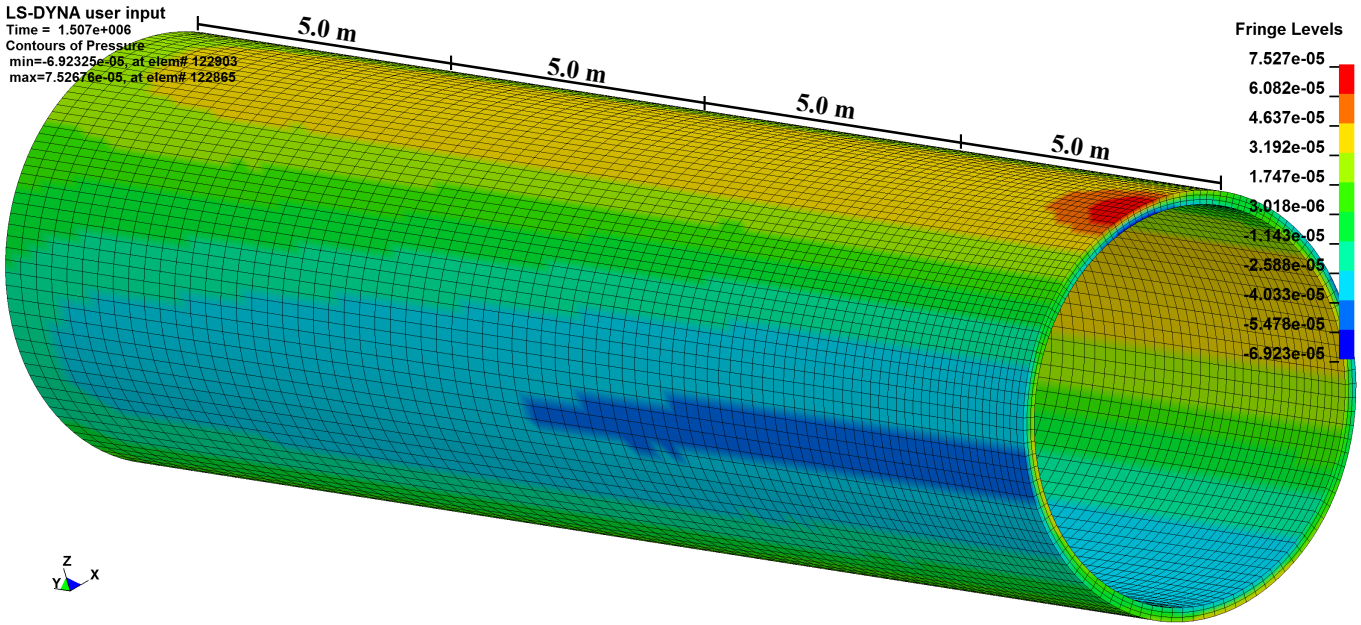

Journal of Performance of Constructed Facilities. Submitted September 20, 2013; accepted January 22, 2014;
posted ahead of print January 25, 2014. doi:10.1061/(ASCE)CF.1943-5509.0000585

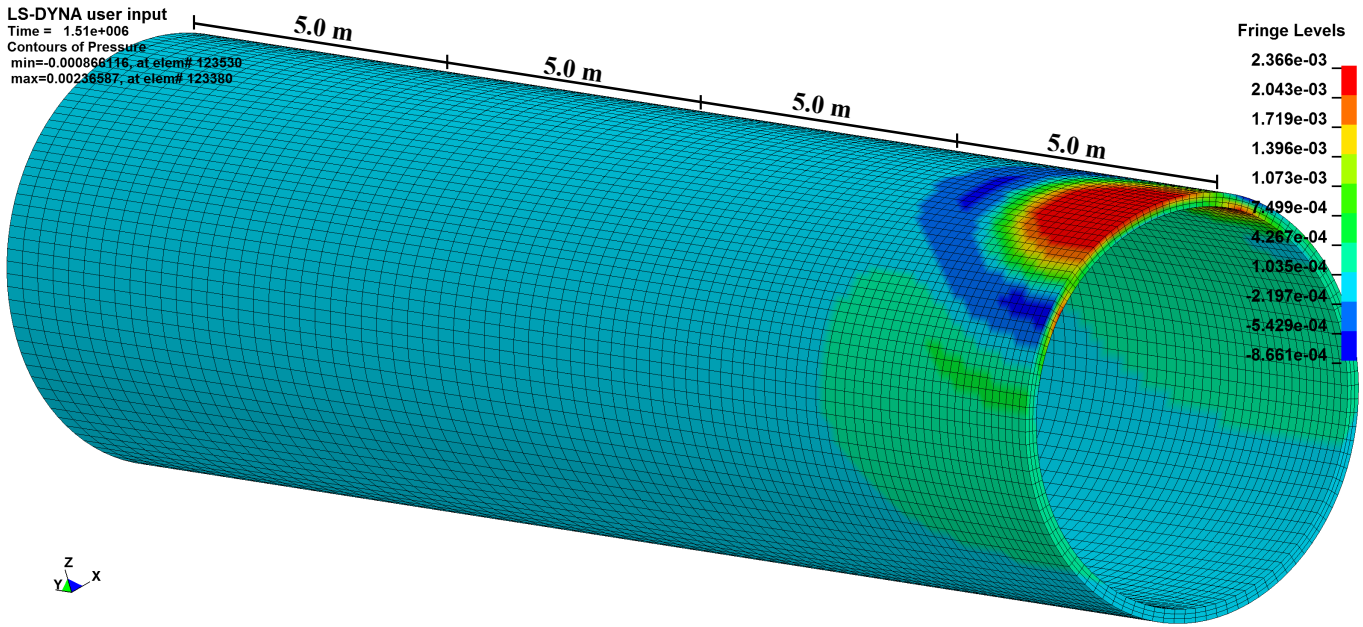

Fig 12(c).pdf

Journal of Performance of Constructed Facilities. Submitted September 20, 2013; accepted January 22, 2014;
posted ahead of print January 25, 2014. doi:10.1061/(ASCE)CF.1943-5509.0000585

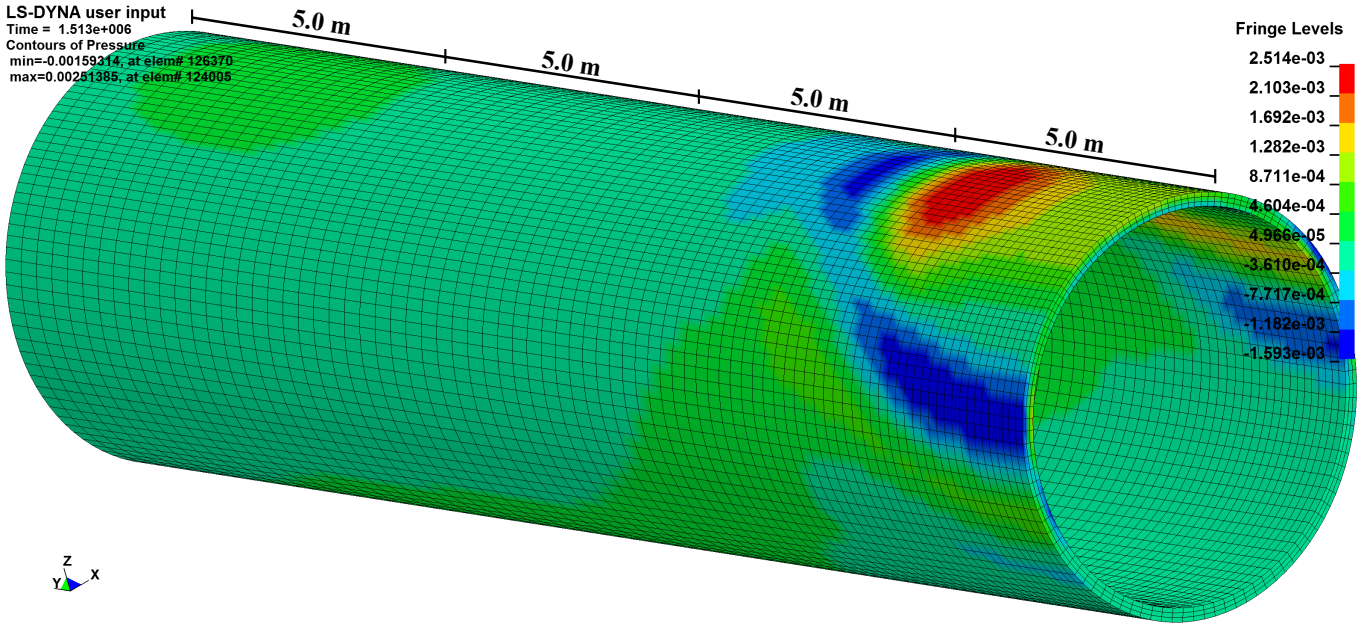

Journal of Performance of Constructed Facilities. Submitted September 20, 2013; accepted January 22, 2014;
posted ahead of print January 25, 2014. doi:10.1061/(ASCE)CF.1943-5509.0000585

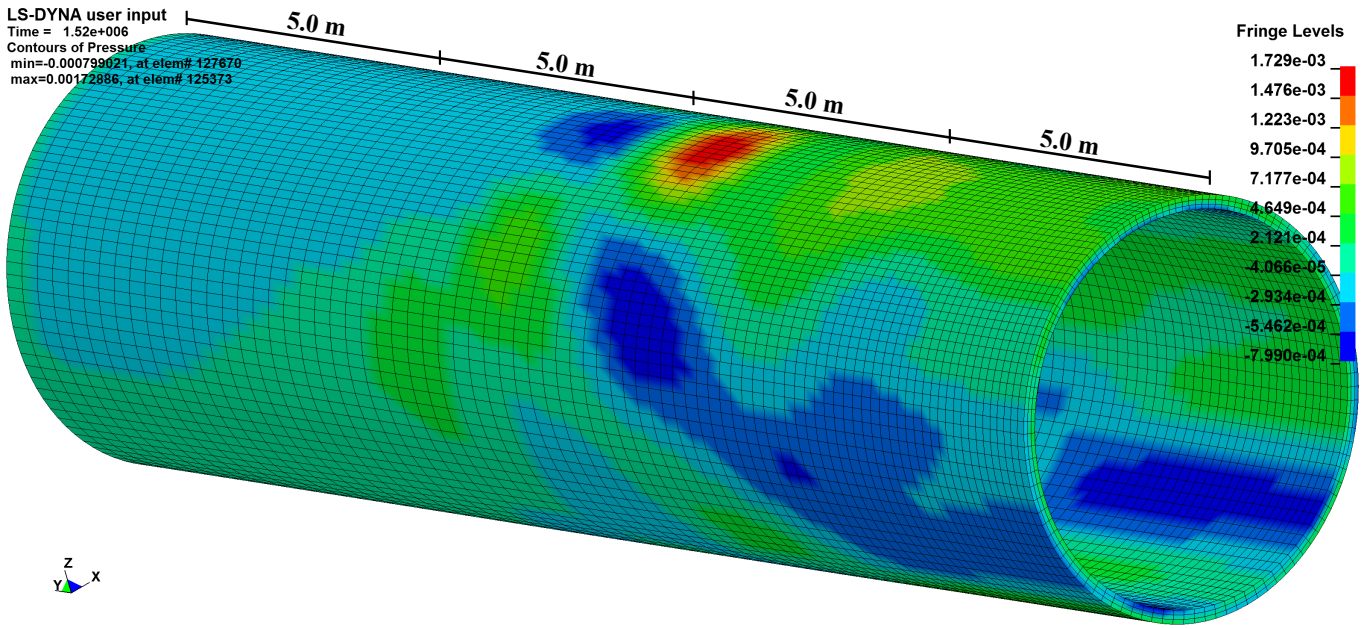

Fig 12(e).pdf

Journal of Performance of Constructed Facilities. Submitted September 20, 2013; accepted January 22, 2014;
posted ahead of print January 25, 2014. doi:10.1061/(ASCE)CF.1943-5509.0000585

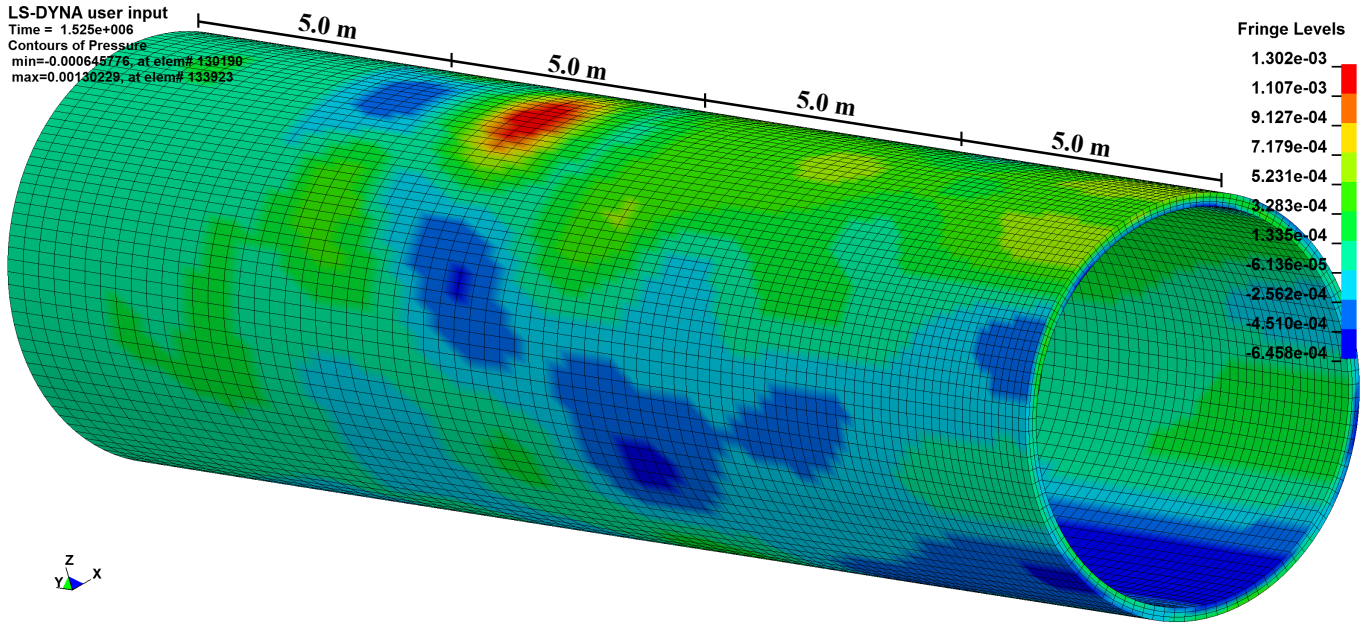

Journal of Performance of Constructed Facilities. Submitted September 20, 2013; accepted January 22, 2014;
posted ahead of print January 25, 2014. doi:10.1061/(ASCE)CF.1943-5509.0000585

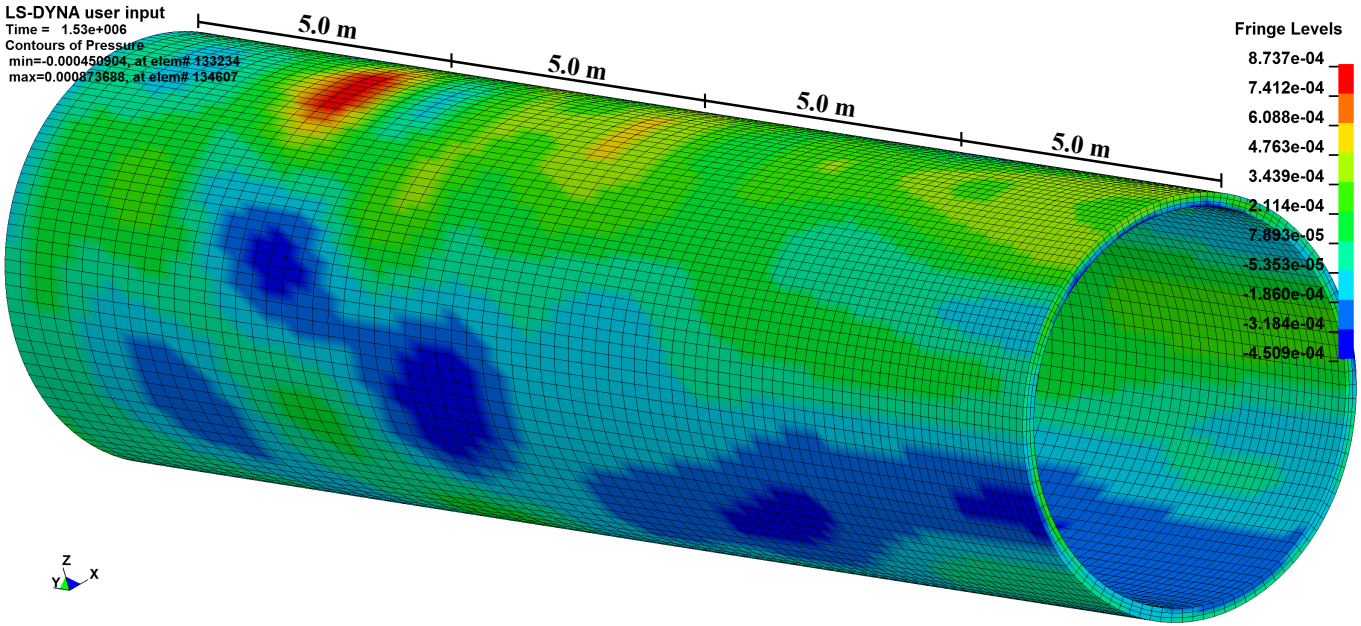

Journal of Performance of Constructed Facilities. Submitted September 20, 2013; accepted January 22, 2014;
posted ahead of print January 25, 2014. doi:10.1061/(ASCE)CF.1943-5509.0000585

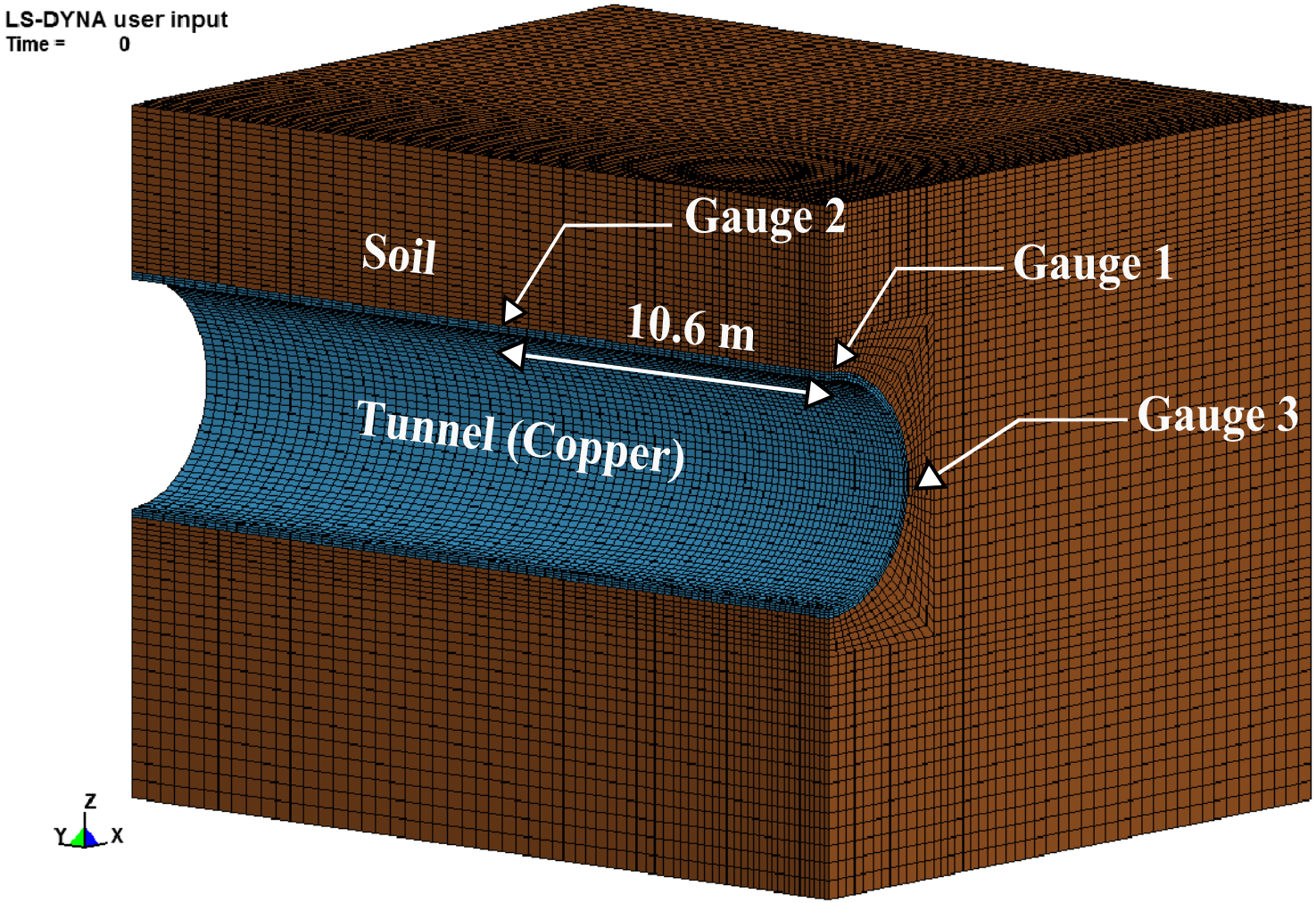

Journal of Performance of Constructed Facilities. Submitted September 20, 2013; accepted January 22, 2014;
posted ahead of print January 25, 2014. doi:10.1061/(ASCE)CF.1943-5509.0000585

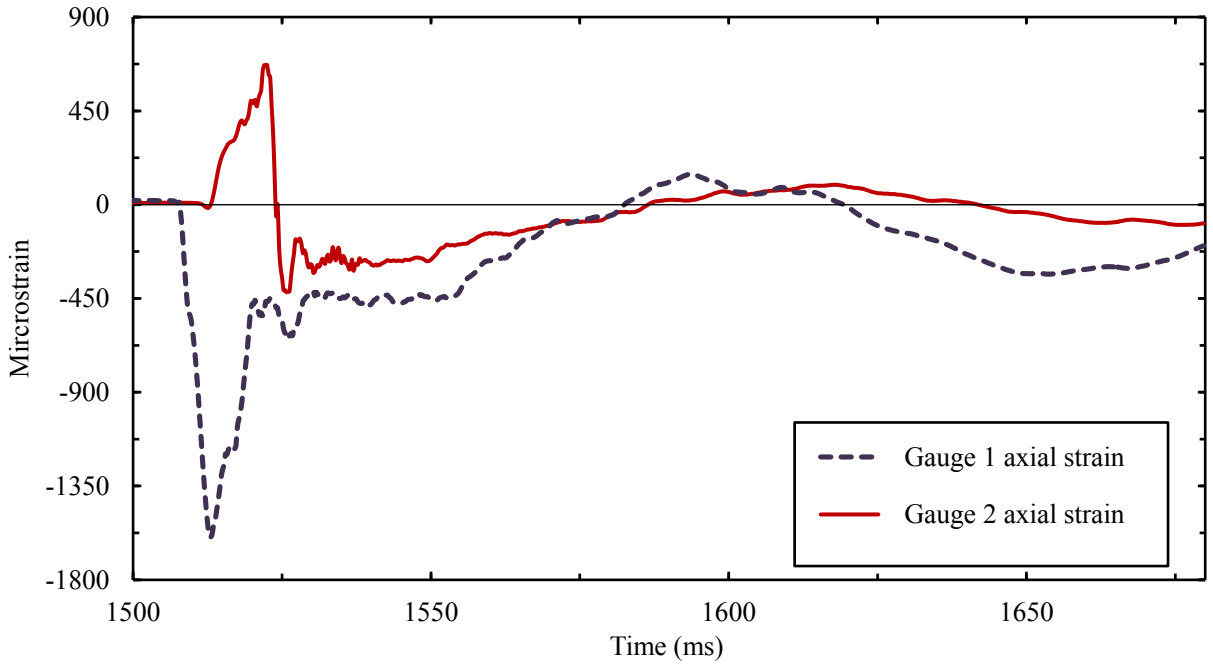

Journal of Performance of Constructed Facilities. Submitted September 20, 2013; accepted January 22, 2014;
posted ahead of print January 25, 2014. doi:10.1061/(ASCE)CF.1943-5509.0000585

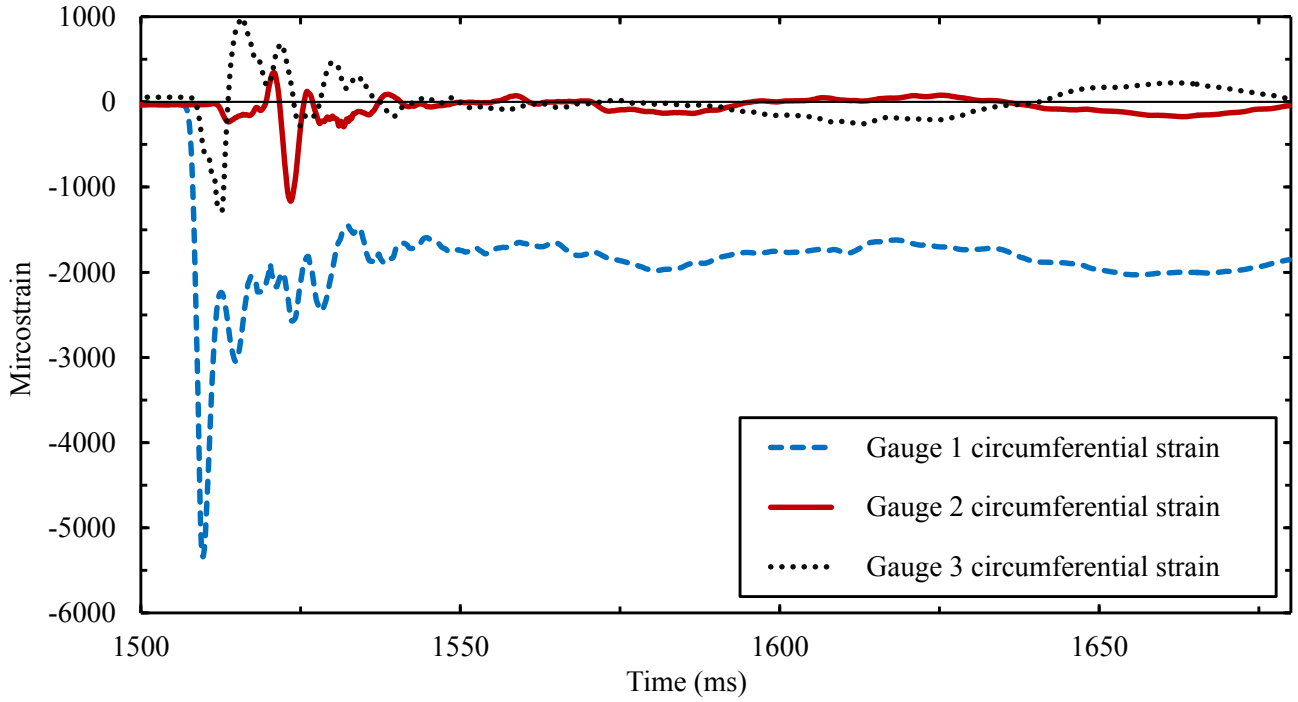

Journal of Performance of Constructed Facilities. Submitted September 20, 2013; accepted January 22, 2014;
posted ahead of print January 25, 2014. doi:10.1061/(ASCE)CF.1943-5509.0000585

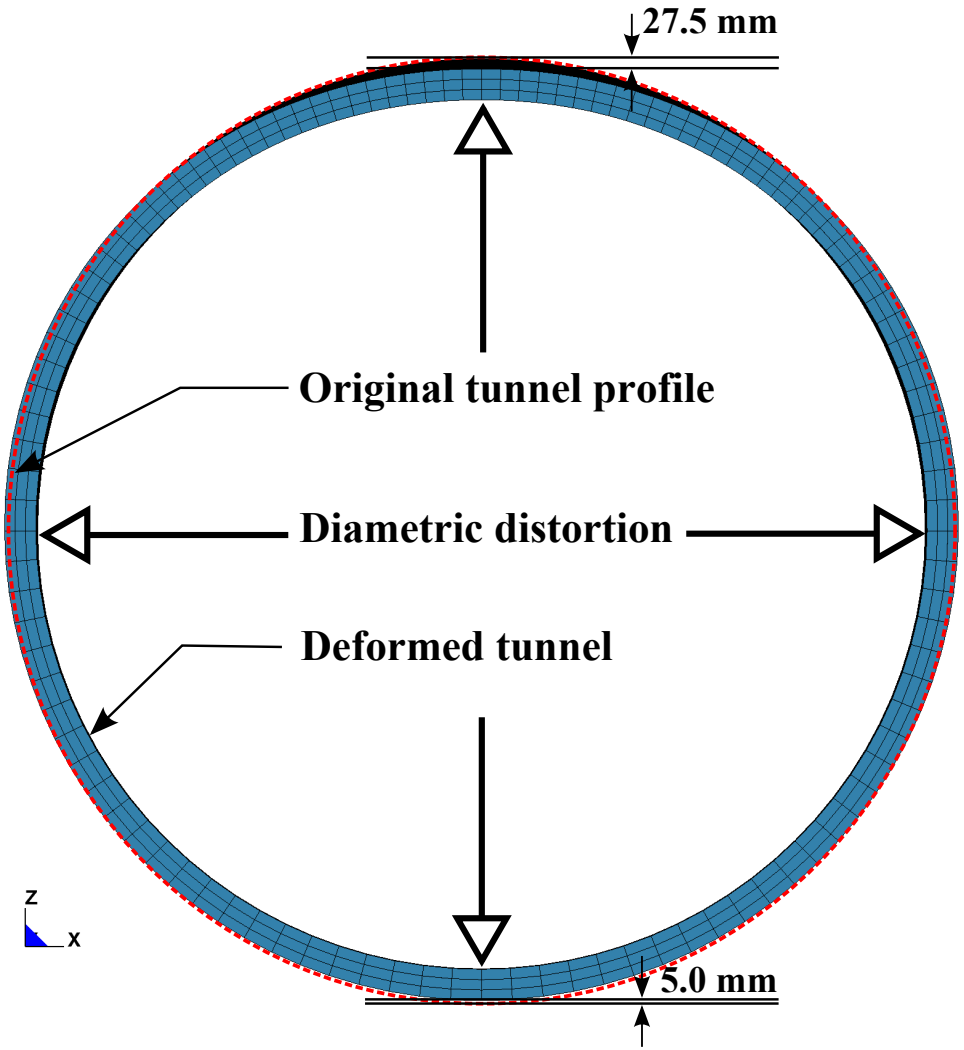

Journal of Performance of Constructed Facilities. Submitted September 20, 2013; accepted January 22, 2014;
posted ahead of print January 25, 2014. doi:10.1061/(ASCE)CF.1943-5509.0000585

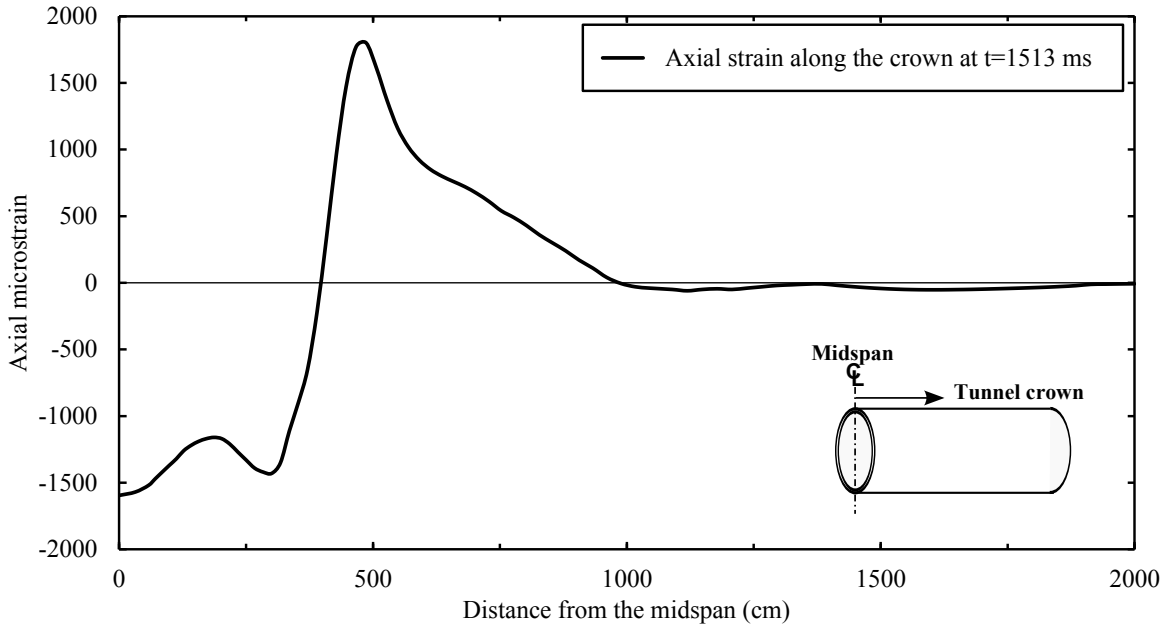

Journal of Performance of Constructed Facilities. Submitted September 20, 2013; accepted January 22, 2014;
posted ahead of print January 25, 2014. doi:10.1061/(ASCE)CF.1943-5509.0000585

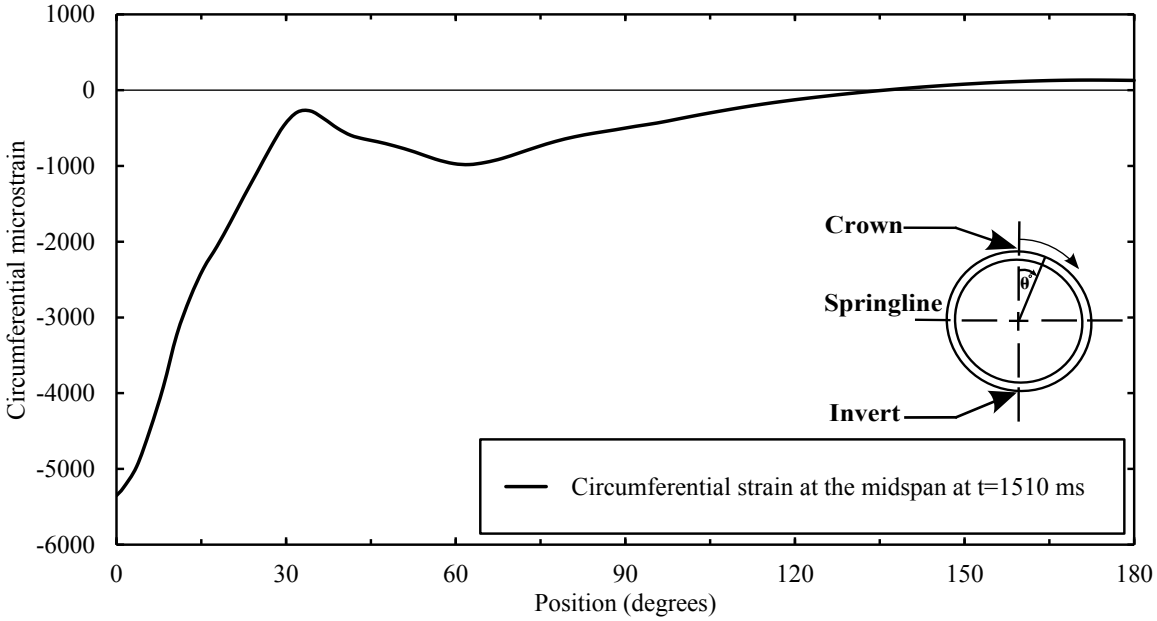

Journal of Performance of Constructed Facilities. Submitted September 20, 2013; accepted January 22, 2014;
posted ahead of print January 25, 2014. doi:10.1061/(ASCE)CF.1943-5509.0000585

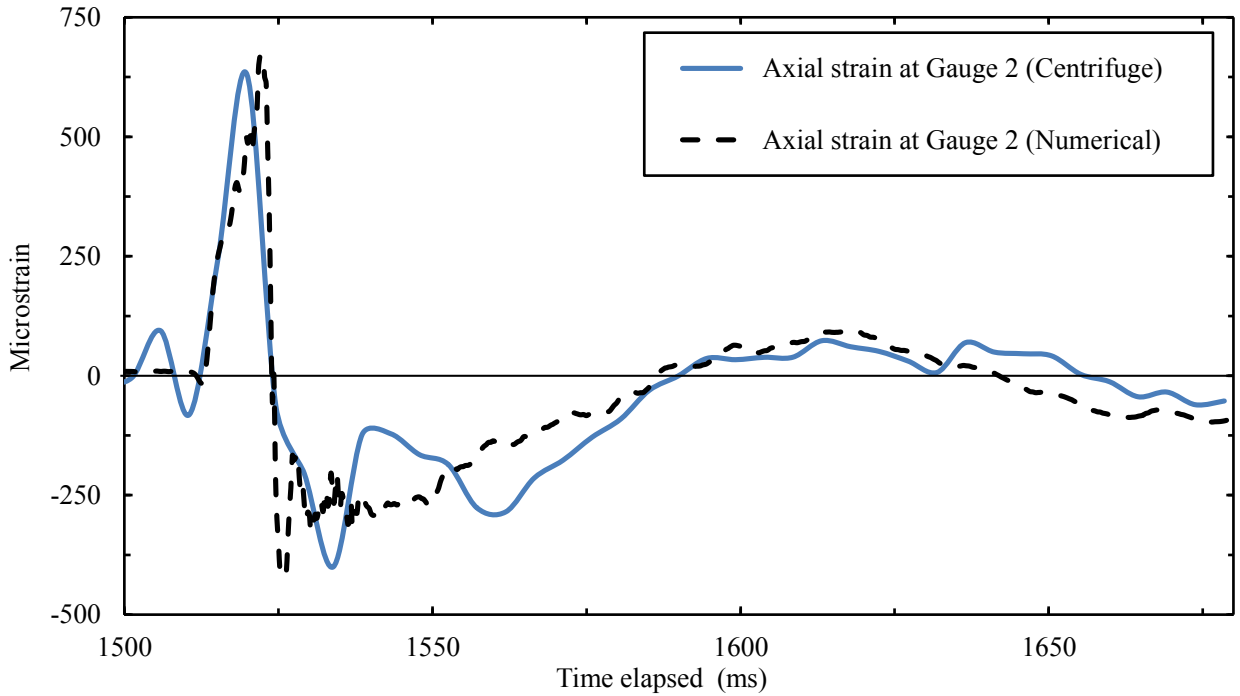

Journal of Performance of Constructed Facilities. Submitted September 20, 2013; accepted January 22, 2014;
posted ahead of print January 25, 2014. doi:10.1061/(ASCE)CF.1943-5509.0000585

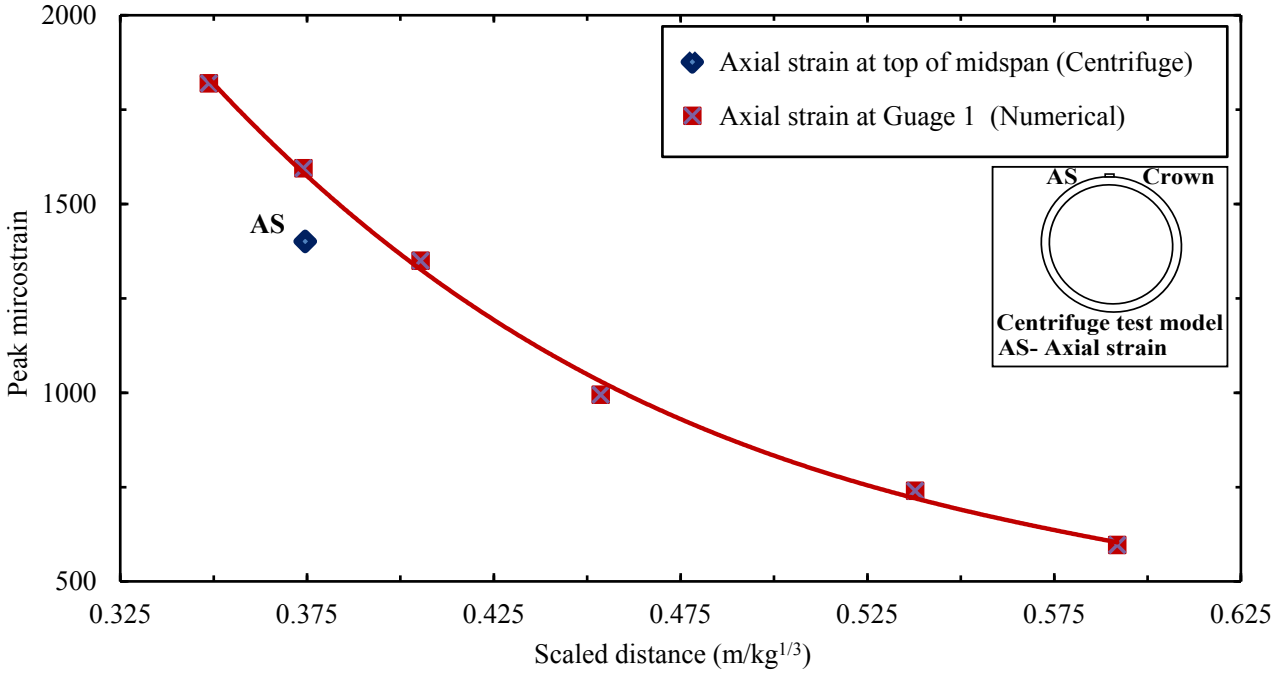

Fig 18(b).pdf

Journal of Performance of Constructed Facilities. Submitted September 20, 2013; accepted January 22, 2014;
posted ahead of print January 25, 2014. doi:10.1061/(ASCE)CF.1943-5509.0000585

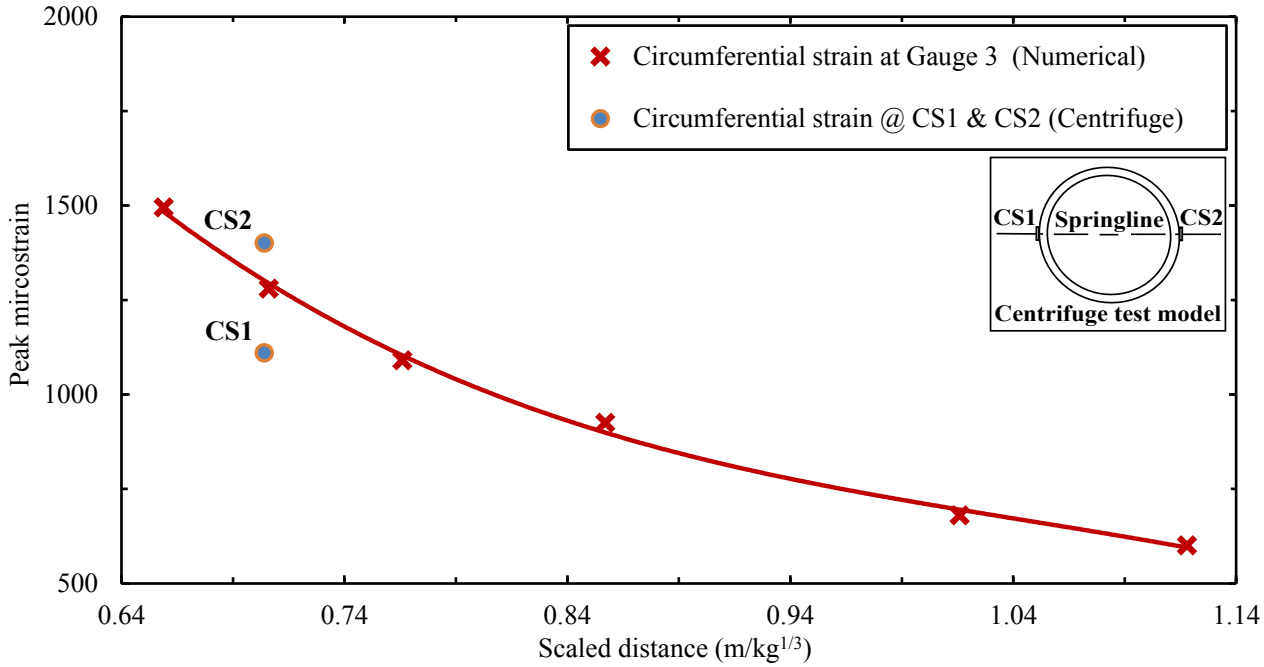

Journal of Performance of Constructed Facilities. Submitted September 20, 2013; accepted January 22, 2014;
posted ahead of print January 25, 2014. doi:10.1061/(ASCE)CF.1943-5509.0000585

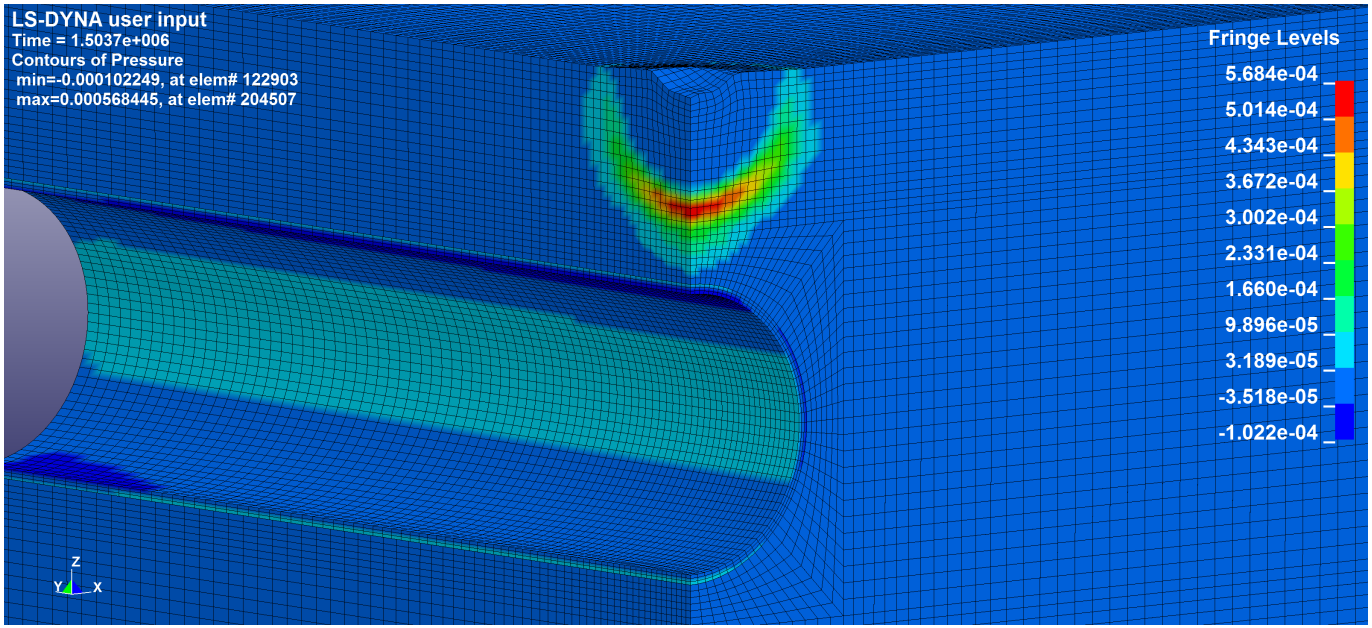

Journal of Performance of Constructed Facilities. Submitted September 20, 2013; accepted January 22, 2014;
posted ahead of print January 25, 2014. doi:10.1061/(ASCE)CF.1943-5509.0000585

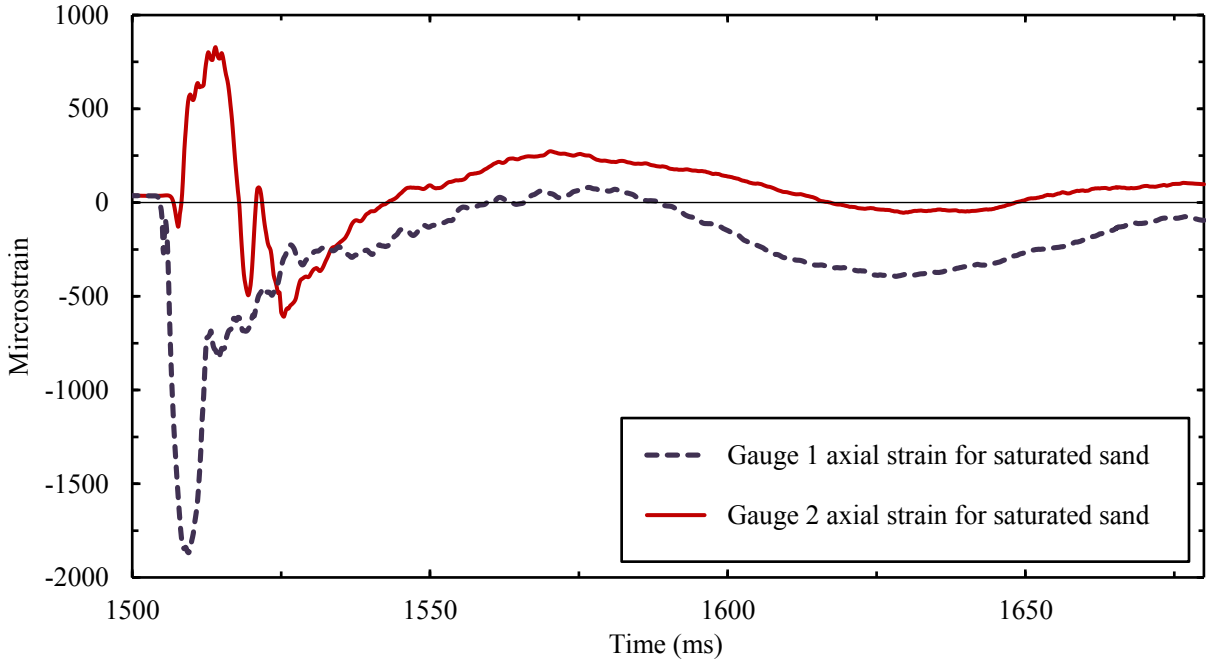

Journal of Performance of Constructed Facilities. Submitted September 20, 2013; accepted January 22, 2014;
posted ahead of print January 25, 2014. doi:10.1061/(ASCE)CF.1943-5509.0000585